

# UNCLASSIFIED

AD NUMBER
ADB215719
NEW LIMITATION CHANGE
TO Approved for public release, distribution unlimited
FROM Distribution authorized to U.S. Gov't. agencies only; Specific Authority; 14 Nov 96. Other requests shall be referred to Commander, Army Medical Research and Materiel Command, Attn: MCMR-RMI-S, Fort Detrick, Frederick, MD 21702-5012.
AUTHORITY
USAMRMC ltr, 4 Dec 2002

THIS PAGE IS UNCLASSIFIED

AD \_\_\_\_\_

CONTRACT NUMBER DAMD17-96-C-6037

TITLE: Low-Power, Low-Cost, High Performance Beamformer for  
Medical Ultrasound Scanners

PRINCIPAL INVESTIGATOR: Thomas E. Linnenbrink,  
Marshall K. Quick, Matthew O'Donnell, Steven R. Freeman

CONTRACTING ORGANIZATION: Q-DOT, Incorporated  
Colorado Springs, Colorado 80907-3579

REPORT DATE: October 1996

TYPE OF REPORT: Final, Phase I

PREPARED FOR: Commander  
U.S. Army Medical Research and Materiel Command  
Fort Detrick, Frederick, Maryland 21702-5012

DISTRIBUTION STATEMENT: Distribution authorized to U.S.  
Government agencies only (specific authority). Other requests  
for this document shall be referred to Commander, U.S. Army  
Medical Research and Materiel Command, ATTN: MCMR-RMI-S,  
Fort Detrick, Frederick, MD 21702-5012.

The views, opinions and/or findings contained in this report are  
those of the author(s) and should not be construed as an official  
Department of the Army position, policy or decision unless so  
designated by other documentation.

# REPORT DOCUMENTATION PAGE

Form Approved  
OMB No. 0704-0188

Public reporting burden for this collection of information is estimated to average 1 hour per response, including the time for reviewing instructions, searching existing data sources, gathering and maintaining the data needed, and completing and reviewing the collection of information. Send comments regarding this burden estimate or any other aspect of this collection of information, including suggestions for reducing this burden, to Washington Headquarters Services, Directorate for Information Operations and Reports, 1215 Jefferson Davis Highway, Suite 1204, Arlington, VA 22202-4302, and to the Office of Management and Budget, Paperwork Reduction Project (0704-0188), Washington, DC 20503.

1. AGENCY USE ONLY (Leave blank)		2. REPORT DATE October 1996		3. REPORT TYPE AND DATES COVERED Final, Phase I (22 Mar 96 - 22 Sep 96)	
4. TITLE AND SUBTITLE Low-Power, Low-Cost, High Performance Beamformer for Medical Ultrasound Scanners				5. FUNDING NUMBERS DAMD17-96-C-6037	
6. AUTHOR(S) Thomas E. Linnenbrink, Marshall K. Quick, Matthew O'Donnell, Steven R. Freeman					
7. PERFORMING ORGANIZATION NAME(S) AND ADDRESS(ES) Q-DOT, Incorporated Colorado Springs, Colorado 80907-3579				8. PERFORMING ORGANIZATION REPORT NUMBER	
9. SPONSORING/MONITORING AGENCY NAME(S) AND ADDRESS(ES) Commander U.S. Army Medical Research and Materiel Command Fort Detrick, Frederick, MD 21702-5012				10. SPONSORING/MONITORING AGENCY REPORT NUMBER	
11. SUPPLEMENTARY NOTES  DTIC QUALITY INSPECTED 2					
12a. DISTRIBUTION / AVAILABILITY STATEMENT Distribution authorized to U.S. Government agencies only (specific authority). Other requests for this document shall be referred to Commander, U.S. Army Medical Research and Materiel Command, ATTN: MCMR-RMI-S, Fort Detrick, Frederick, MD 21702-5012.				12b. DISTRIBUTION CODE 1 4 NOV 1996	
13. ABSTRACT (Maximum 200)  <p>Ultrasonic imaging is the preferred method for noninvasive tissue examination and real-time evaluation of blood flow. Foreign items (e.g., radiolucent shrapnel) embedded in the body can also be imaged. While this would greatly aid combat field medics and civilian emergency medical technicians, current ultrasound scanners are too large, heavy, and power consumptive for battery operation. Major scanner functions' size, weight, and power must be significantly reduced for portable operation.</p> <p>The beamformer dynamically focuses, apodizes, and steers both transmitted and received ultrasonic waveforms. Modern beamformers typically utilize an analog-to-digital (ADC) at each element, followed by digital memory and signal processing circuitry. The beamformer is amenable to the extensive size, weight, and power reduction possible using charge-coupled device (CCD) technology.</p> <p>A full beamformer chip was specified under the Phase I program. Its critical elements were designed and fabricated. This beamformer will yield a system with performance comparable to the current commercial state of the art, at roughly 10% of the size, weight, and power of a digital approach. Limitations of the CCDs were evaluated and shown to have negligible effect on image quality. Under Phase II, a complete multichannel beamformer chip will be designed and fabricated.</p>					
14. SUBJECT TERMS ultrasound, beamformer, charge-coupled device, dynamic focus, beam steering, imaging, blood flow, delay line				15. NUMBER OF PAGES 41	
				16. PRICE CODE	
17. SECURITY CLASSIFICATION OF REPORT Unclassified	18. SECURITY CLASSIFICATION OF THIS PAGE Unclassified	19. SECURITY CLASSIFICATION OF ABSTRACT Unclassified	20. LIMITATION OF ABSTRACT Limited		

## FOREWORD

Opinions, interpretations, conclusions and recommendations are those of the author and are not necessarily endorsed by the U.S. Army.

N/A Where copyrighted material is quoted, permission has been obtained to use such material.

Julie Where material from documents designated for limited distribution is quoted, permission has been obtained to use the material.

N/A Citations of commercial organizations and trade names in report do not constitute an official Department of the Army endorsement or approval of the products or services of these organizations.

N/A In conducting research using animals, the investigator(s) adhered to the "Guide for the Care and Use of Laboratory Animals," prepared by the Committee on Care and Use of Laboratory Animals of the Institute of Laboratory Resources, National Research Council (NIH Publication No. 86-23, Revised 1985).

N/A For the protection of human subjects, the investigator(s) adhered to policies of applicable Federal Law 45 CFR 46.

N/A In conducting research utilizing recombinant DNA technology, the investigator(s) adhered to current guidelines promulgated by the National Institutes of Health.

N/A In the conduct of research utilizing recombinant DNA, the investigator(s) adhered to the NIH Guidelines for Research Involving Recombinant DNA Molecules.

N/A In the conduct of research involving hazardous organisms, the investigator(s) adhered to the CDC-NIH Guide for Biosafety in Microbiological and Biomedical Laboratories.

Thomas E. Linnenbrink

Thomas E. Linnenbrink *ea*

Principal Investigator

October 2, 1996

Date



## Table of Contents

Section	Page
Report Documentation Page (SF 298) .....	2
Foreword .....	3
Table of Figures .....	5
1.0 Executive Summary .....	6
2.0 Introduction .....	7
3.0 Phase I Technical Objectives .....	10
4.0 Technical Discussion .....	11
4.1 Requirements .....	11
4.2 Beamformer .....	14
4.2.1 Technical Approach .....	14
4.2.2 Complementary Delay Line .....	15
4.2.3 Crossbar Switch Functional Description .....	17
4.2.4 Quad Sampler .....	21
4.2.5 Delay Line Control .....	24
4.2.6 Prototype Element Fabrication .....	27
4.3 Potential Performance Limiting Factor .....	29
4.3.1 Charge Transfer Efficiency Effects .....	30
4.3.2 Dynamic Range .....	34
4.3.3 Power Consumption .....	34
4.4 Phase II Development Plan .....	35
5.0 Conclusions .....	38
Appendix Phase II Work Plan Detail .....	39
List of Personnel Who Work on the Program .....	41

## Table of Figures

Figure	Page
1. Ultrasonic Imaging System Block Diagram .....	8
2. Typical Digital Front-End Processor .....	9
3. Proposed Sampled Analog Front-End Processor .....	9
4. Man-Packable Scanner Configuration .....	11
5. System Specification .....	13
6. Sampled Analog (CCD / CMOS) Beamformer Chip .....	14
7. Crossbar Switch .....	16
8. Complementary Delay Line .....	16
9. Monotonic Switching of Complementary Delay Line .....	17
10. CCD / CMOS Complementary Delay Line .....	18
11. Crossbar Switch .....	19
12. Crossbar Switch in Straight Mode .....	20
13. CCD Crossbar Switch in Cross Mode .....	21
14. Quad Sampler Structure .....	22
15. Operation of Quad Sampler .....	23
16. Control Sequences .....	25
17. Geographical Offsets .....	25
18. Modified Control Circuitry .....	26
19. Bump Clock Generator .....	27
20. Beamformer Test Chip Mask .....	28
21. Crossbar Switch Test Element .....	29
22. Complementary Delay Line Test Element .....	30
23. Quad Sampler Test Element .....	31
24. Fourier Transform of Wire Target .....	33
25. Wires, No CTE Effects .....	33
26. Wires, CTE = 0.995 .....	33
27. Cyst Phantom, No CTE Effects .....	33
28. Cyst Phantom, CTE = 0.995 .....	33
29. Phase II Work Plan .....	35
30. Phase II Option Work Plan .....	35
31. Phase II Work Plan Detail .....	39
32. Phase II Demonstration Option Work Plan Detail .....	40

## 1.0 Executive Summary

Ultrasonic imaging is the method of choice for noninvasive examination of tissue and real-time evaluation of blood flow. It is also capable of imaging foreign bodies, such as radiolucent shrapnel, especially in the abdomen and chest. These functions would significantly aid a combat medic operating in the zone of close combat (or a civilian counterpart operating at an accident site) if a suitable backpackable instrument existed.

A backpackable ultrasound array imaging system must be compact, lightweight, electrically efficient and mechanically rugged, yet provide excellent image quality and color flow sensitivity. Under this SBIR program, we investigated a sampled analog beamformer to dramatically reduce the size, weight and power consumption of a portable array imaging system. The key technical issue is to develop a specific beamforming architecture approximating the image quality and flow sensitivity of current commercial systems.

Clinically, the system must be able to find and assess abdominal injury, especially free fluid. In addition, it should be useful for other trauma applications, as well as possible obstetrics and gynecological examinations using an endovaginal probe. Sensitive color flow images and duplex Doppler measurements are needed to differentiate soft tissue from blood pools and identify ruptured blood vessels. The quality of such measurements is directly related to the instantaneous dynamic range of the beamformer. Consequently, the system must provide an instantaneous dynamic range comparable to the current commercial state of the art.

Phase I of this project:

- ♦ defined a set of requirements for the beamformer that will yield a system with performance comparable to the current commercial state of the art,
- ♦ developed a manufacturable CCD delay line that will meet these requirements,
- ♦ fabricated critical elements of the CCD delay line, and
- ♦ developed a control algorithm that will maintain a tight focus at all image depths.

Simulations of the Phase I design predicts:

- ♦ power consumption will be 10% of conventional digital techniques, which makes portable, battery powered operation feasible,
- ♦ dynamic range will be adequate for sensitive color flow images and duplex Doppler measurements, and
- ♦ the charge transfer efficiency of the CCDs will have negligible effect on image quality.

Phase II of this project will yield a full beamformer chip suitable for use in a portable, battery powered ultrasound imager. This phase includes design, two passes at fabrication, and test. Under an optional demonstration phase, a set of Phase II beamformer chips will be configured into a full beamformer and coupled to an actual transducer probe to capture data in real time, for off-line processing and display.

A complete backpackable ultrasound imaging system based on the beamformer chips will be developed as a Phase III effort.



## 2.0 Introduction

Ultrasonic imaging is the method of choice for noninvasive examination of tissue and real-time evaluation of blood flow. It is also capable of imaging foreign bodies, such as radiolucent shrapnel, especially in the abdomen and chest. These functions would significantly aide a combat medic operating in the zone of close combat (or a civilian counterpart operating at an accident site) if a suitable instrument existed. However, present diagnostic ultrasound scanners are large, heavy, require hundreds of watts of power, and are not particularly amenable to portable operation. (One new scanner draws so much power that it cannot be plugged into a conventional wall socket!) Figure 1 diagrams a conventional ultrasonic imaging system. This real-time phased-array system typically employs a linear or curved array of piezoelectric transducers operating in a frequency range of roughly 1 MHz to 10 MHz, depending on the penetration depth required and the desired resolution. Typical modern front-end processor circuitry comprises predominantly digital circuitry, as shown in Figure 2. Transmission waveforms are usually developed as square waves in the beamformer which are subsequently filtered or smoothed into approximately sinusoidal waveforms by the transducer itself and its driver. Alternatively, the transmission waveform is a series of digital words which are converted to an analog signal by a digital-to-analog converter (DAC) prior to driving the transducer. The transducer converts the electronic signal to an ultrasound waveform which is directed into the body under observation. Body tissue reflects the ultrasound wave which the transducer converts back to an electric signal. This signal is amplified and scaled with a time-gain compensation amplifier (TGC). The TGC compensates for depth-dependent attenuation of the ultrasound signal in tissue. Next the received signal is converted to a series of digital words with an analog-to-digital converter (ADC) prior to beamforming.

A typical digital beamformer performs in-line data storage, dynamic focusing, steering, and apodization functions digitally. It comprises random access memory (RAM), digital signal processors (DSPs), microprocessors, and other digital logic components. Both the transmitted *and* received waveforms are focused, steered, and apodized to support confocal operation. Digital beamforming offers excellent images and Doppler flow data at the expense of size, weight, and power consumption in the processor. An individual ADC (and DAC) is required for every transducer element. Current transducers usually employ 32 to 192 elements. Advanced transducers may employ more than 1,000 elements to enhance resolution and reduce phase aberration. These digital waveforms must be individually delayed, apodized (by multiplying with a weighting function), and summed. For a typical 128-element system these functions require more than 30 billion mathematical operations per second! Fortunately, the functions readily map into parallel processors. However, the combined size and power is formidable, especially when considered for application in portable, man-packed equipment for use by combat medics in the zone of close combat.

The proposed sampled-analog beamformer shown in Figure 3 provides the same functionality as the typical digital processor described above, but at roughly 10% of its size, weight, 10% power consumption, and cost. The proposed sampled-analog front-end beamformer will be realized in high-speed charge-coupled device (CCD) technology combined on the same integrated circuit chip with analog and digital CMOS devices. While this effort addressed only the beamformer functions, in the future the entire front-end processor may be integrated with advanced CCD/CMOS technology. It will even be possible for the entire front-end processor to be moved out of the system into the transducer probe, resulting in additional savings in size, power consumption, and cost.



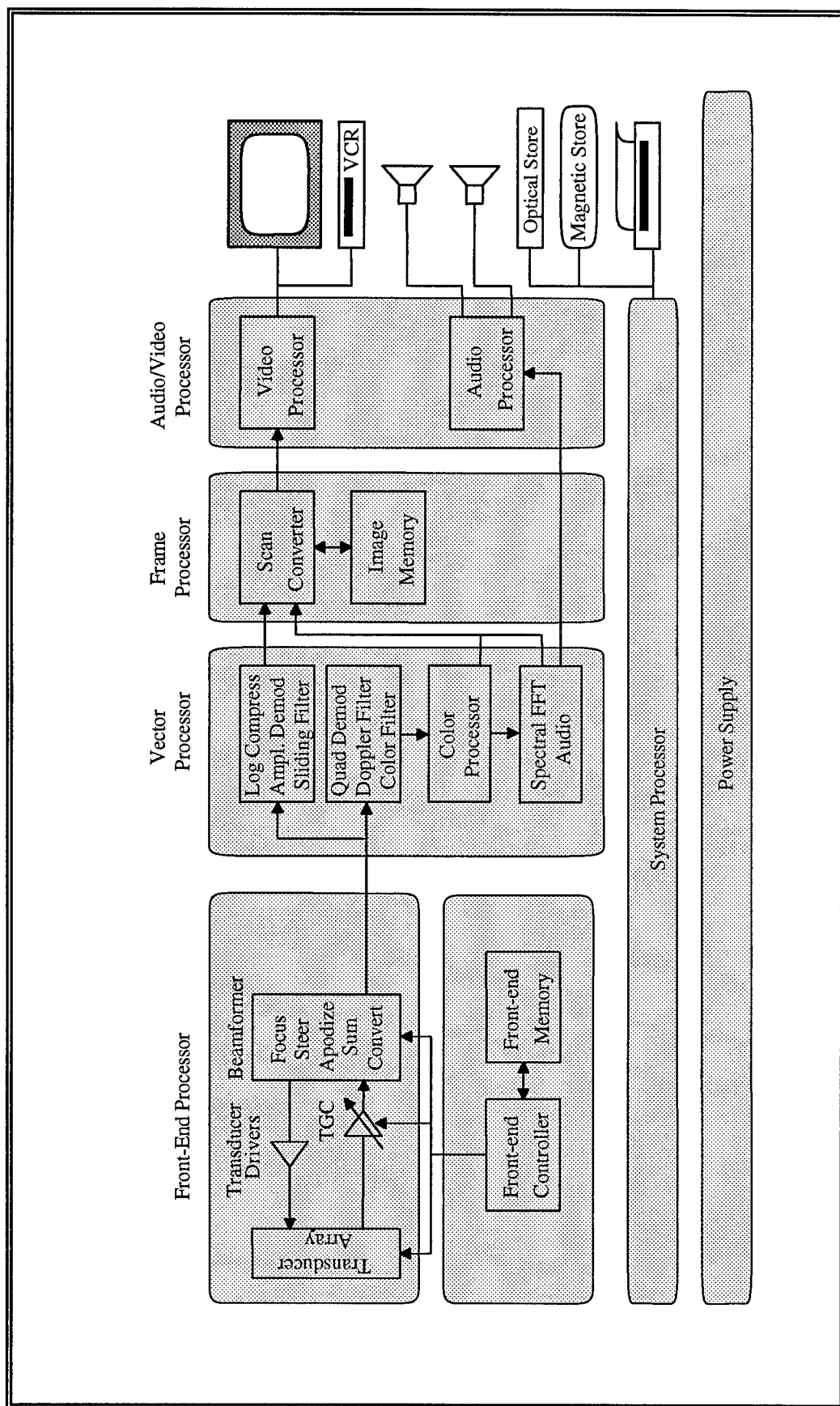


Figure 1: Ultrasonic Imaging System Block Diagram

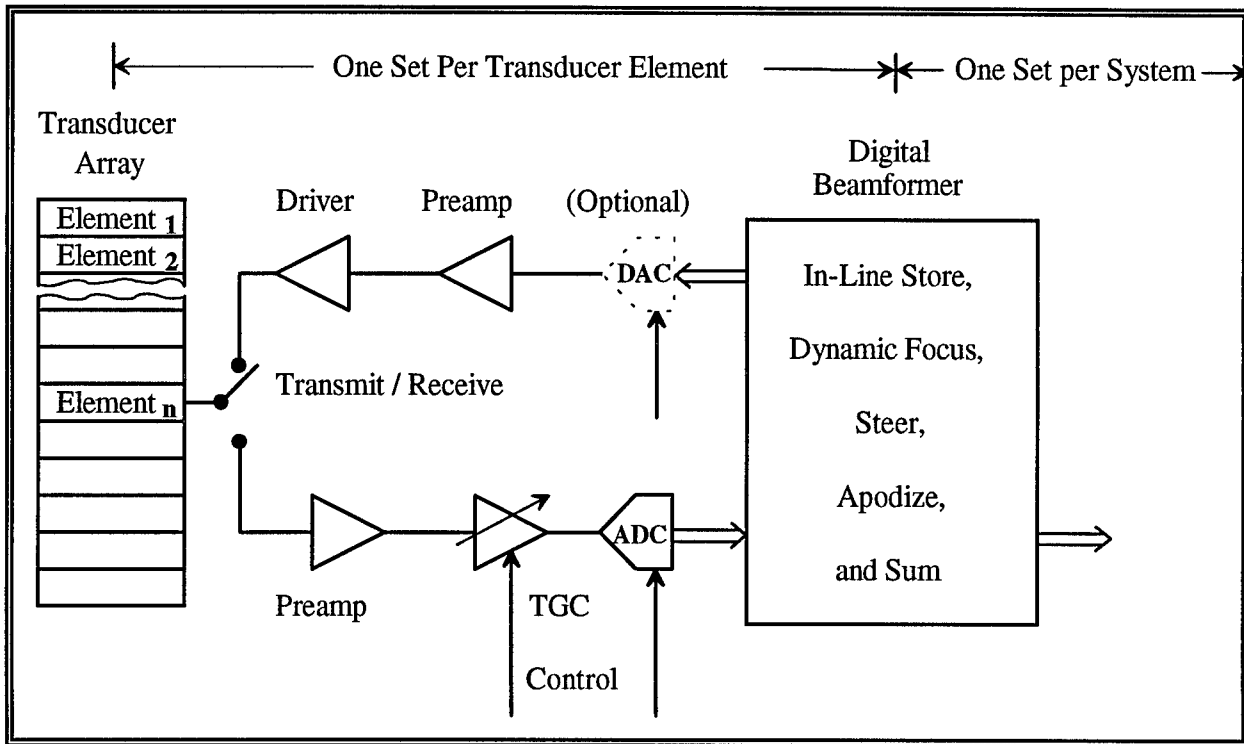


Figure 2: Typical Digital Front-End Processor

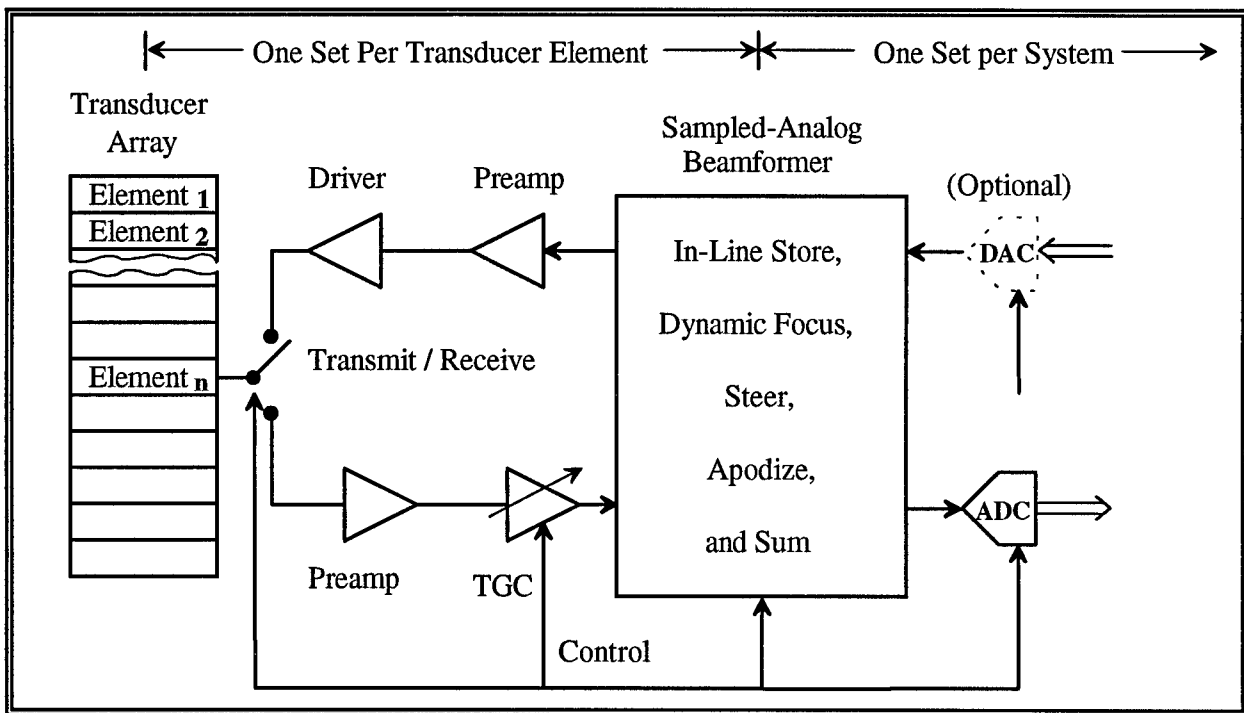


Figure 3: Proposed Sampled Analog Front-End Processor

### 3.0 Phase I Technical Objectives

The major objective of the Phase I effort is to assess the technical feasibility of developing a high-performance beamformer for a compact, low-power, low-cost, ultrasonic scanner which meets both TRP and industry requirements for use by combat medics in the zone of close combat *and* by civilian emergency medical technicians (EMTs) at the scene of an emergency. Specific objectives include:

- 1) Define the target system specification with TRP technical personnel *and* with commercial medical ultrasound equipment manufacturers to sharpen Q-DOT's focus on real-world requirements;
- 2) Synthesize candidate ultrasonic beamformers using advanced CCD/CMOS technology to meet the refined specification;
- 3) Analyze elements of the candidate beamformers to discover their performance limitations;
- 4) Refine the candidate beamformer architectures based on analysis of the elements, estimate the performance of the refined beamformers, and review results with TRP *and* industry technical personnel;
- 5) Structure a work plan to develop the resulting beamformers; and
- 6) Briefly document the Phase I effort, focusing on its results.



## 4.0 Technical Discussion

A backpackable ultrasound array imaging system must be compact, lightweight, electrically efficient and mechanically rugged, yet provide excellent image quality and color flow sensitivity. A conceptual configuration is shown in Figure 4. The bulk of the electronic scanner is housed in a backpack. Wireless (RF) links connect the scanner to a local (e.g., 50 foot radius) combat medic and a remote radiologist. The combat medic wears a pod the size of a package of cigarettes (on his forearm or thigh). The pod is linked via cable to the hand-held probe and via a wireless link to the backpack. The pod contains the beamformer, a color display, an audio link to the radiologist, and batteries. The medic can then probe independently or with guidance from the radiologist. In this SBIR program, we are investigating a sampled analog beamformer to dramatically reduce the size, weight and power consumption of a portable array imaging system. The key technical issue is to develop a specific beamforming architecture approximating the image quality and flow sensitivity of current commercial systems.

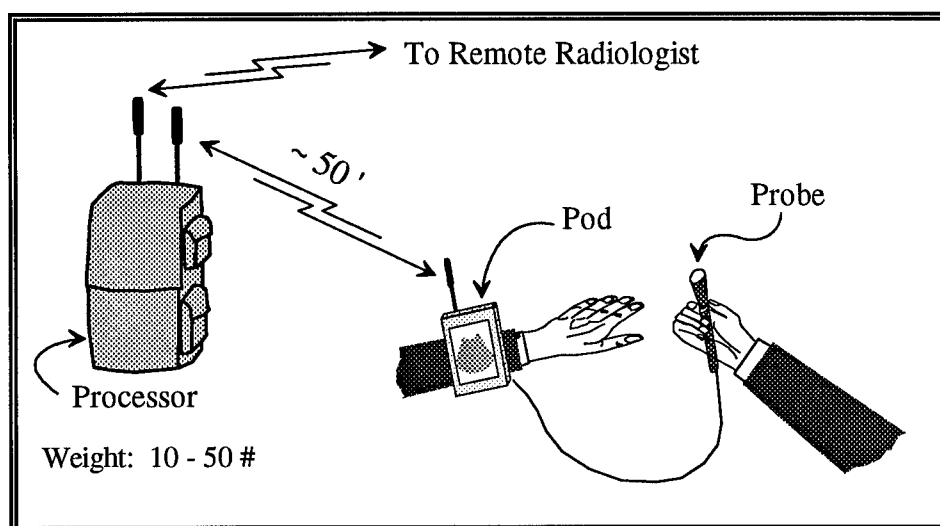


Figure 4: Man-Packable Scanner Configuration

## 4.1 Requirements

Clinically, the system must be able to find and assess abdominal injury, especially free fluid. In addition, it should be useful for other trauma applications, as well as possible obstetrics and gynecological examinations using an endovaginal probe. Consequently, the system should be able to image with both phased arrays (element size comparable to about half a wavelength at the center frequency) and convex/linear arrays (element size comparable to a wavelength at the center frequency) operating over a frequency range of about 2.5 - 10 MHz. Since the finest spatial resolution theoretically possible is not a key requirement for these applications, a 64-channel beamformer is sufficient. Relatively large, 1-dimensional convex and linear arrays can image with this channel count, yielding spatial and contrast resolution comparable to the current commercial state of the art. For phased arrays, the spatial resolution will be about half that of current commercial systems. Since phased arrays will only be used for a limited number of trauma applications, this resolution loss will be acceptable if the system is highly portable.

Sensitive color flow images and duplex Doppler measurements are needed to differentiate soft tissue from blood pools and identify ruptured blood vessels. The quality of such measurements is directly

related to the instantaneous dynamic range of the beamformer. Consequently, the system must provide an instantaneous dynamic range comparable to the current commercial state of the art.

Given these requirements, the system specification presented in Figure 5 was developed. The system must operate over a frequency range from 2.5 - 10 MHz. The beamformer also must be able to generate a 90-degree sector image with focusing to a depth of  $500 \lambda$  to accommodate all probe types. High quality transmit beamforming is assured with the combination of amplitude apodization (accurate to 1 part in 64) and precise time delay accuracy ( $\lambda/32$ ). On transmit, signals output from the sampled analog beamformer can be used to drive low impedance amplifiers exciting individual array elements. A very short set-up time is provided so that high PRF Doppler is possible.

On receive, full dynamic focusing and apodization are needed to maintain the contrast and spatial resolution required for all possible applications. Again, both amplitude apodization and precise time delay accuracy are provided for optimal beamforming. A sophisticated control system is also required to maintain a tight focus at all image depths. On each channel, time delays can be independently updated once every wavelength. This permits a fully dynamic aperture with an  $f$ number as low as unity. Again, a very short set-up time is provided for the receive beamformer so that high PRF Doppler is possible.

For a 64-channel beamformer, the maximum acoustic dynamic range (ratio of the mainbeam strength to average sidelobe levels) is about 72 dB. This means the instantaneous electronic dynamic range must at least equal this level for sensitive Doppler measurements. The target for dynamic range, therefore, is specified as 70 - 75 dB. It may be possible to achieve an 80 dB electronic dynamic range. If such a level can be reached, then color flow images, as well as conventional real-time B-Scans, will only be limited by the acoustics of the imaging system. This is the current state of the art for commercial array scanners.

In the next section, the specific sampled analog architecture designed to deliver these target specifications is described in detail.

<i>Specification</i>	<i>Proposed</i>	<i>Acceptable</i>	<i>Desired</i>
<b>General</b>			
Center Frequency	2.5 - 10 MHz	x	
Steering Range	$\pm 45^\circ$	x	
Focus Range (Pulse Echo)	2 - 500 $\lambda$	x	
<b>Transmit Mode</b>			
Dynamic Range (from beamformer chip)	40 dB	x	
Apodization	64 Levels	x	
Coarse Delay (for Steering)			
Range	48 $\lambda$	x	
Resolution	$\lambda$	x	
Fine Delay (for Focus and Steering)			
Range	8 $\lambda$	$\lambda$	$\lambda \dagger$
Resolution	$\lambda / 32$	x	
Set-up Time	3 $\mu$ s	x	0 $\ddagger$
<b>Receive Mode</b>			
Frequency Deviation	$\pm 0.4 f_0$	x	
Input Signal	2 V p-p	x	
Output Signal	4 mA p-p	x	
System Dynamic Range	60 - 70 dB	70 - 75 dB	80 dB
Channel-to-Channel Cross Talk	- 40 dB	x	-45 to -50 dB
Apodization			
Range	64 Levels	x	
Update Interval	$\lambda$	x	
Coarse Delay (for Steering)			
Range	48 $\lambda$	x	
Resolution	$\lambda$	x	
Update	1 / Scan	x	
Fine Delay (for Dynamic Focus and Steering)			
Range	8 $\lambda$	x	
Resolution	$\lambda / 32$	x	
Update Interval	$\lambda$	x	
Programming	3 $\mu$ s	x	0 $\ddagger$

$\dagger$  Theoretically, you only need  $\lambda$  length fine delays since the focus is fixed. Spec is quoted this way because the same structure is used for transmit and receive.

$\ddagger$  For color flow, there should be *no* setup or programming delays for repetitive firings along the *same* beam line.

Figure 5: System Specification

## 4.2 Beamformer

### 4.2.1 Technical Approach

The beamformer architecture diagrammed in Figure 6 is the preferred candidate for implementation in advanced CMOS/CCD technology. Each of the 32 channels of the beamformer contains the same circuit up to the final summation ( $\Sigma$ ) and partial beam output. (This output will be summed with the outputs of other beamformer chips to form a complete beam.) After the signal from an individual transducer element is conditioned by its preamp and TGC, it is presented to an input channel of the beamformer. The signal is sampled in quadrature. That is, samples are acquired at  $0^\circ$ ,  $90^\circ$ ,  $180^\circ$ , and  $270^\circ$  of the sampling clock. In this example, the sampling clock ( $f_s$ ) operates at eight times the center frequency ( $f_s = 8 f_o$ ), or each sample spans  $1/8$ th of a center frequency wavelength ( $\lambda/8$ ). Quadrature sampling effectively increases the sampling rate to  $32 f_o$  and the resolution to  $\lambda/32$ . Quad samplers cycle through their four samplers in the same order *but with different initial conditions*. Thus,  $\lambda/32$  resolution is maintained among all channels in the beamformer as well as among all beamformer chips in the system. Individual samplers will be realized with Q-DOT's proven diode-cutoff sampler.

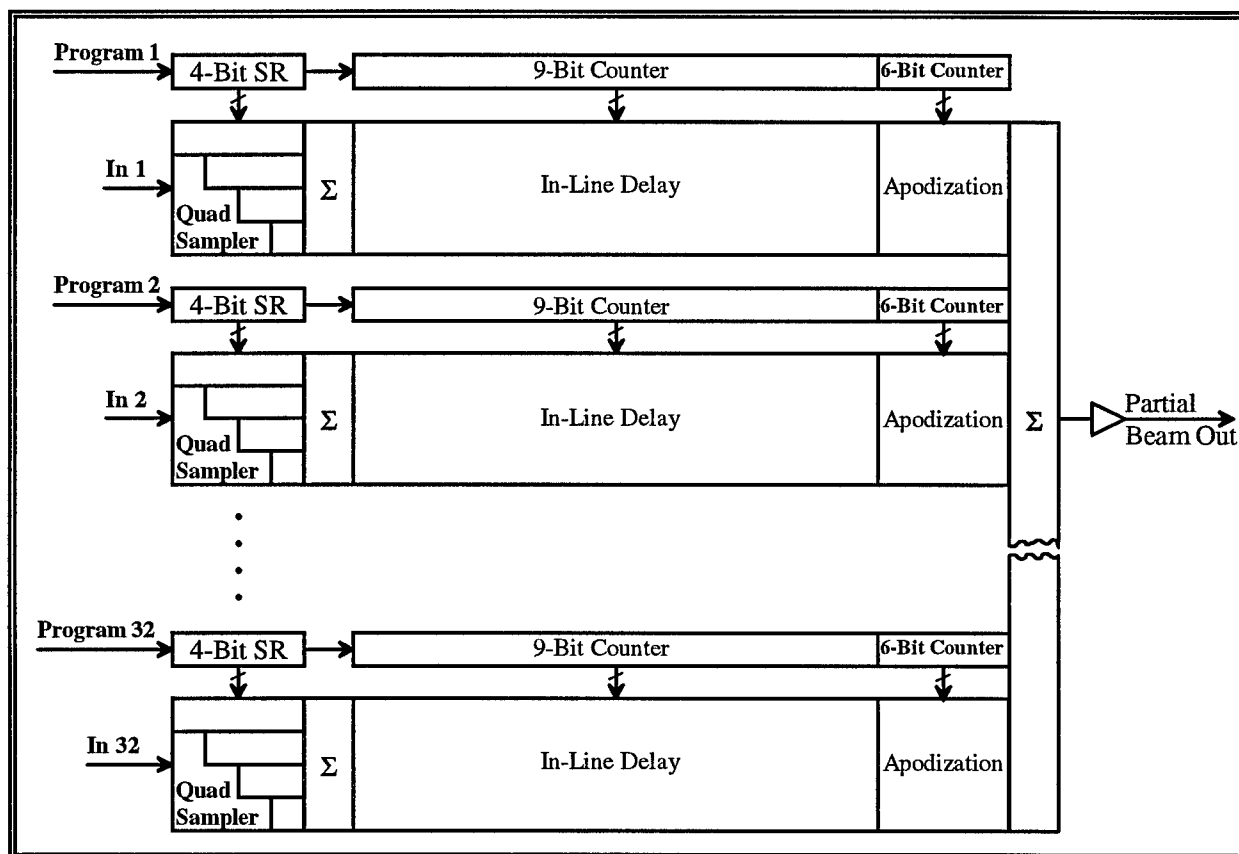


Figure 6: Sampled Analog (CCD / CMOS) Beamformer Chip

With time resolution established in the quad sampler, groups of three samples may be summed for the remaining operations. This reduces the number of delay stages required to span  $56\lambda$  by a factor of four. Since the in-line delay circuitry dominates the beamformer, and since the delay stages are nearly minimum size, total chip area is reduced by a factor of at least three. Since the number of acceptable chips

per wafer varies approximately inversely as the square of chip area, the yield of acceptable chips per wafer is increased by about a factor of 10 (with corresponding cost reduction). The reduction in sampling clock rate from  $32 f_s$  to  $8 f_s$  combined with the reduction in delay stages reduces power dissipation in the in-line delay by a factor of 16. Power dissipation in the apodizer, output summation, and output amplifier is reduced by a factor of four, benefiting only from the change in sampling clock rate.

The in-line delay comprises a series of nine, binary-weighted stages. Each stage can add twice as much net delay as the previous stage. The first stage can insert a delay of zero or  $\lambda/8$ , the second stage zero or  $\lambda/4$ , etc., to the last stage which can insert zero or  $32\lambda$ . The composite delay ranges from zero to  $63.875\lambda$  in  $\lambda/8$  steps. The composite delay can be dynamically incremented or decremented in  $\lambda/8$  steps by incrementing its control counter *while maintaining a monotonic time sequence of signal samples*. (Details are presented in Section 4.2.2. This single in-line delay section, together with the quad sampler, is used for both beam steering and dynamic focusing.

After it is delayed appropriately, each signal is apodized by attenuating its amplitude. The apodizer provides 64 gain ranges spanning a minimum gain of zero to a maximum gain of  $63/64$  in  $1/64$  increments. Apodization can be dynamically changed in single level steps by incrementing its 6-bit control counter. Apodization is performed with a charge-mode multiplying digital-to-analog converter (MDAC) which Q-DOT is currently employing in several developmental circuits.

After apodization, charge samples from all 32 channels on the chip are summed and converted to an equivalent output current by a CMOS amplifier. The synchronous, sampled nature of the data is maintained in this process resulting in a stepped (zero order hold) signal. Current outputs from all beamformer chips are readily summed with an operational amplifier (not shown).

The beamformer is programmed via individual serial ports for each channel. Initial conditions for the quad sampler shift register (SR), the in-line delay counter, and the apodization counter are loaded prior to each ultrasound pulse.

The previous discussion addresses the beamformer as it is configured to receive the reflected ultrasound pulse. The same fundamental components are used for transmit beamforming. For transmission, all the inputs are tied together and driven from an on-chip waveform generator (not shown). After apodization, outputs are switched from the common summation circuitry to individual output buffers (not shown). The same physical chip can perform both transmit and receive functions, but are typically dedicated to one use in a system. It is also possible to design a beamformer to operate bidirectionally, effectively providing both functions on the same chip.

#### 4.2.2 Complementary Delay Line

The key to the beamformer's small size, low power, ease of programming, and monotonic time sequence is the innovative complementary delay line. As will become apparent, a key element in the complementary delay line is a crossbar switch. Shown in Figure 7, the crossbar switch has two states. In the straight path state, its two inputs are connected in parallel to its two outputs. In the crossed path state, the two input signals are crossed before they are individually applied to the two outputs. No other states are permitted. The symbol for a crossbar switch is also shown.



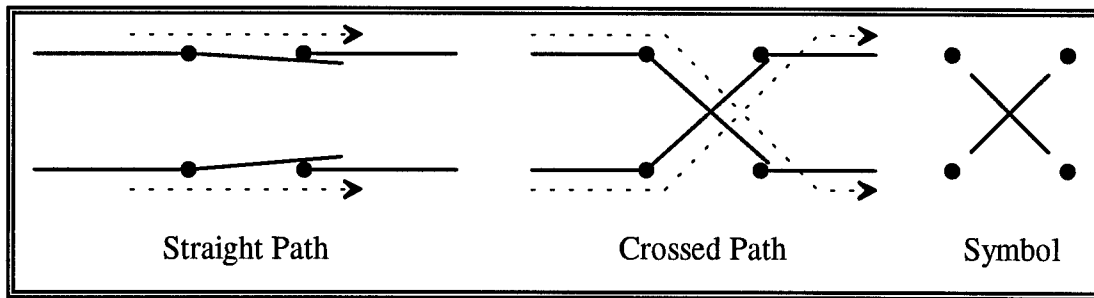


Figure 7: Crossbar Switch

A three-stage complementary delay line is shown in schematic form in Figure 8. The input signal is split into two equal parts which are delayed equally to the first stage. One signal is routed to the short path (1A) and the other to the long path (1B). Path 1A is  $\Delta t$  long, while 1B is  $2\Delta t$  long, resulting in a Stage 1 net delay of  $\Delta t$ . The Stage 1 signals are next routed to the Stage 2 delays, 2A and 2B, via a crossbar switch. The choices are (1A  $\rightarrow$  2A and 1B  $\rightarrow$  2B) or (1A  $\rightarrow$  2B and 1B  $\rightarrow$  2A). Stage 2 provides delays of  $\Delta t$  and  $3\Delta t$ , resulting in a net delay of  $2\Delta t$ . Similarly, the Stage 2 output signals are linked to Stage 3 via another crossbar switch. After the last stage, one of the last stage signals is linked to the output while the other is discarded.

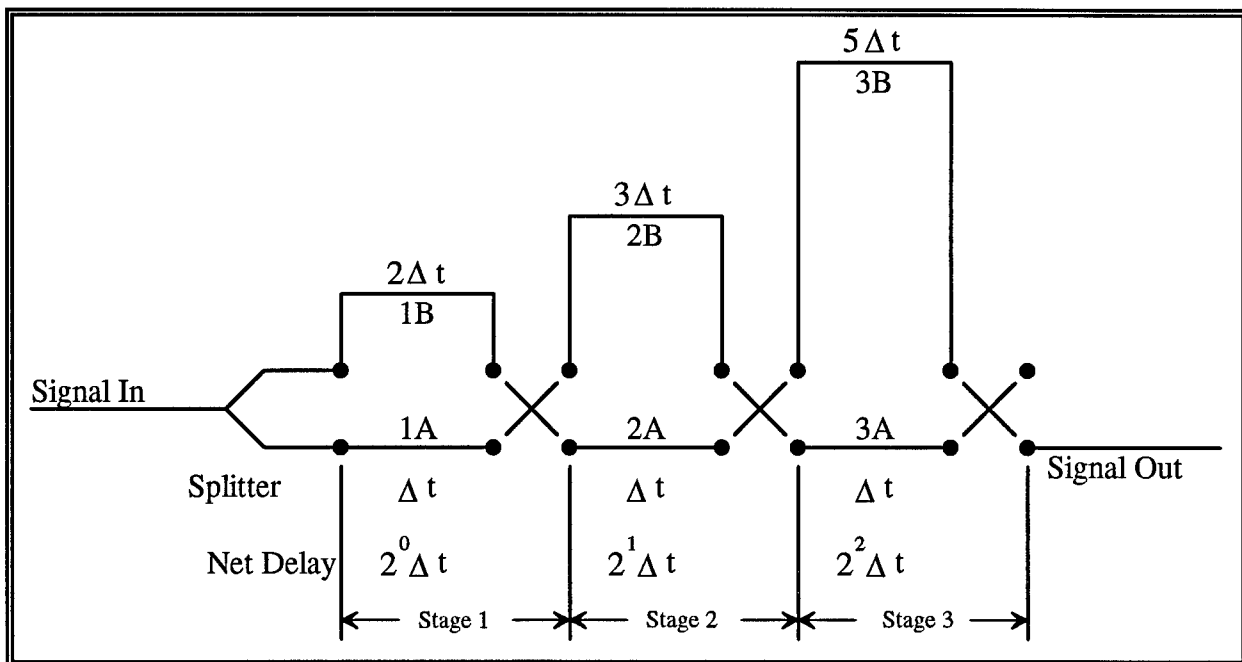


Figure 8: Complementary Delay Line

Monotonicity of the time sequence is diagrammed in Figure 9. For convenience, time is graphed in discrete steps of  $\Delta t$ . The oldest time increment is labeled A, the next oldest B, etc. Both paths of the complementary in-line delay diagrammed in Figure 8 are shown as branches from a common starting point at  $t_0$ . In the initial condition before switching, elements 1A, 2B, and 3A are in the output path while 1B, 2A, and 3B are in the complement path. The total delay from input to output is  $5\Delta t$ . The time increments present in each path are labeled. Then the Stage 1 increments are swapped to increase the output delay by

$\Delta t$ . (The swap is done by toggling all crossbar switches.) If these elements are swapped instantaneously, they will carry the signal present in them before the swap to their new path. The result of this instantaneous swap is shown in the "After Switching" portion of Figure 9. Note that an extra L increment has been added to the output sequence as the output path was lengthened. The complement path is missing an L increment. However, *both paths remain monotonic*. Monotonicity is maintained for all possible  $\pm \Delta t$  switching. The impact of repeating or skipping a time increment is minimized by keeping  $\Delta t$  relatively small, in this case  $\lambda/8$ .

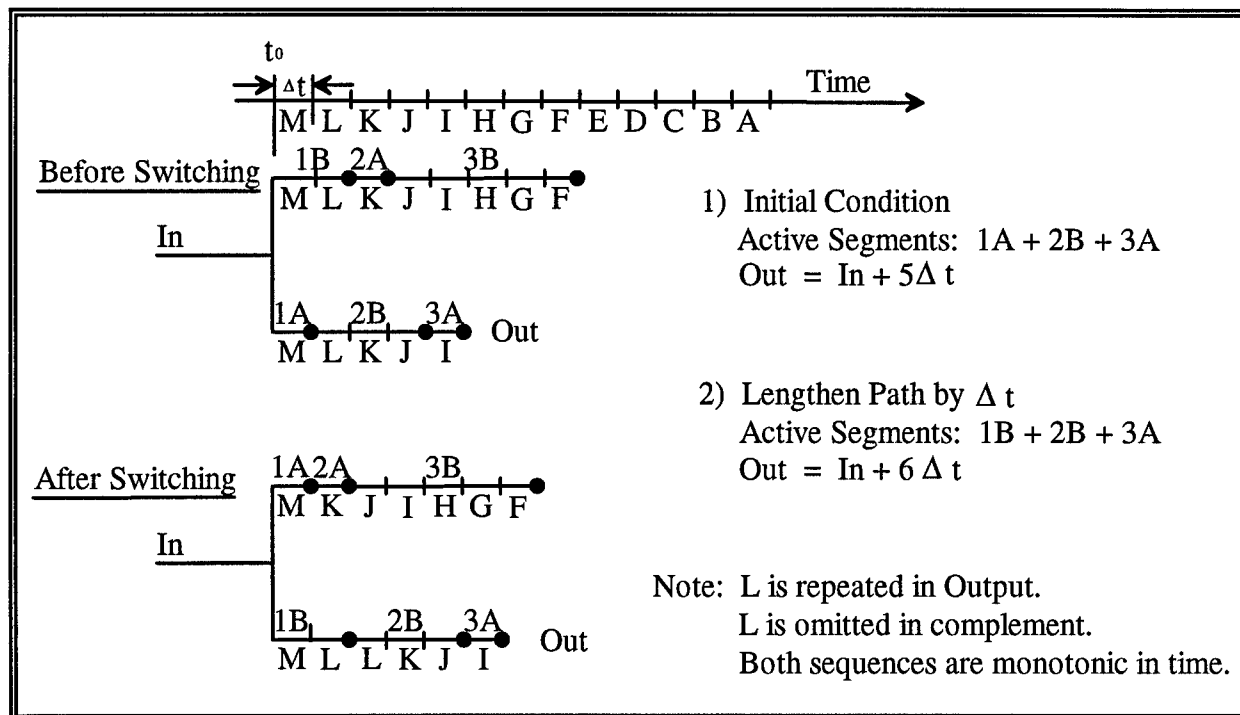


Figure 9: Monotonic Switching of Complementary Delay Line

A CCD/CMOS version of this three-stage complementary delay line is sketched in Figure 10. CCD technology is well suited to the complementary delay line architecture because all signals reside in discrete charge packets and move synchronously through the delay line one data cell at a time. Therefore, the crossbar switching is both instantaneous and lossless. Delay elements corresponding to the A and B paths are shaded. Paths through the three crossbar switches are indicated by distinctive arrows. Nonprogrammable charge packet movement is indicated with short arrows. The input charge is split precisely by implementing precision splitting techniques developed at Q-DOT. The innovative crossbar switch was developed under this program.

#### 4.2.3 Crossbar Switch Functional Description

The crossbar switch is the key element in the complementary delay line. The crossbar switch simultaneously accepts two charge packets, and under digital control, either passes the two packets in parallel to a pair of outputs (straight mode), or it swaps the two packets at the output (cross mode).

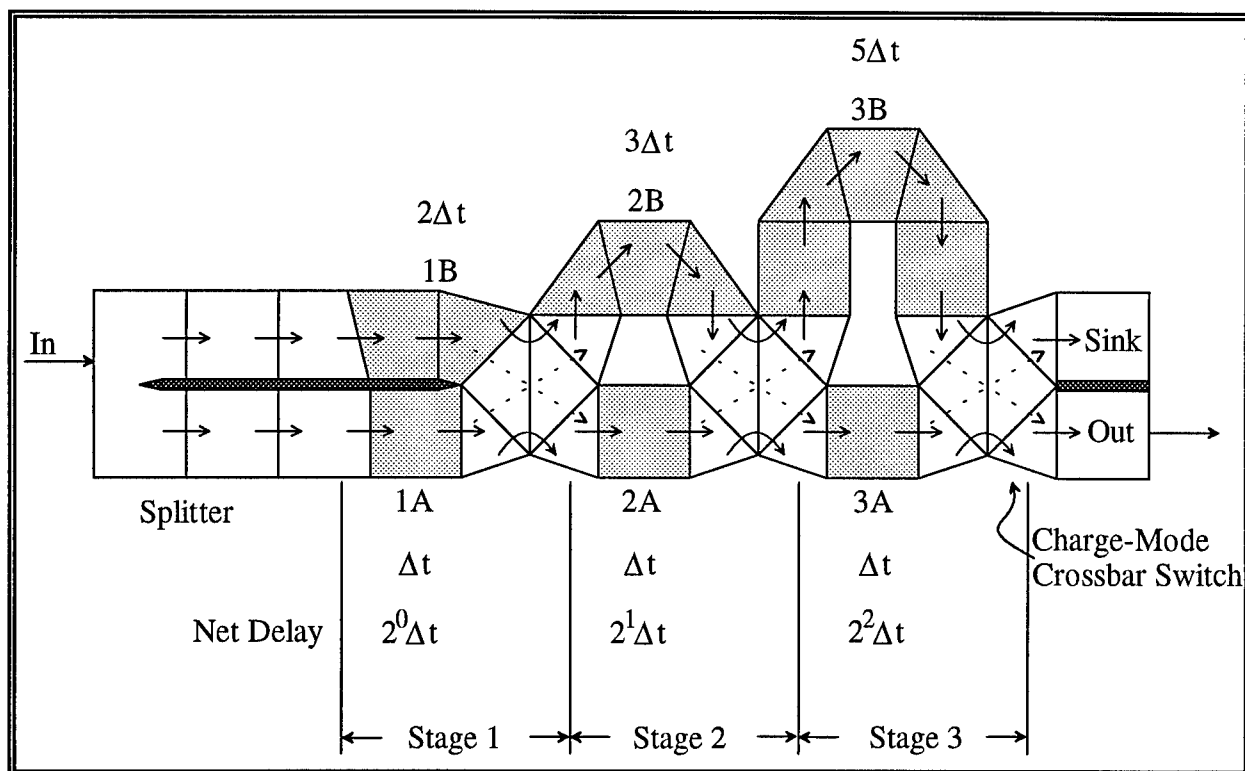


Figure 10: CCD / CMOS Complementary Delay Line

The selected structure for the CCD implementation of the crossbar switch is shown in Figure 11a, where the CCD gate outlines are labeled with the name of a clocking signal connected to the gate. The six gates on the right are each connected through a CMOS multiplexer (switch) to either of the two clocks indicated. The effect of changing the switch position is to swap the upper and lower clocks. The clocks applied to the crossbar switch are shown in Figure 11b.

The gates outlined in Figure 11a are conductors placed on the top surface of the silicon, with a thin layer of insulator separating the gate from the silicon. Charge in the form of electrons is free to move within an area known as a channel which lies under the CCD gates. When a gate is in the on state (positive), the negative mobile charge in the channel is attracted to the gate and is held in a potential well immediately underneath the gate. If two adjacent gates are both on, and the gates adjacent to that pair are off, the potential well will be under both on gates, and the charge packet will be coupled under both gates. The packet of charge held in the joint potential well is passed along a channel by manipulating the clock voltages applied to the gates. The packet of charge is moved forward by turning the upstream gate off, while simultaneously turning the downstream gate on, which has the net effect of moving the charge forward by one gate position, where it will be held until the next clocking event. A structure known as a diode-cutoff sampler (not shown) generates a packet of charge proportional to the input voltage at a sample time, and a floating diffusion sense circuit (not shown) is used to produce a voltage proportional to the size of the charge packet. This ability to store and move signal samples provides a means of delaying the signal samples in time, which makes the CCD technology ideal for programmable delay lines in the beamformer.

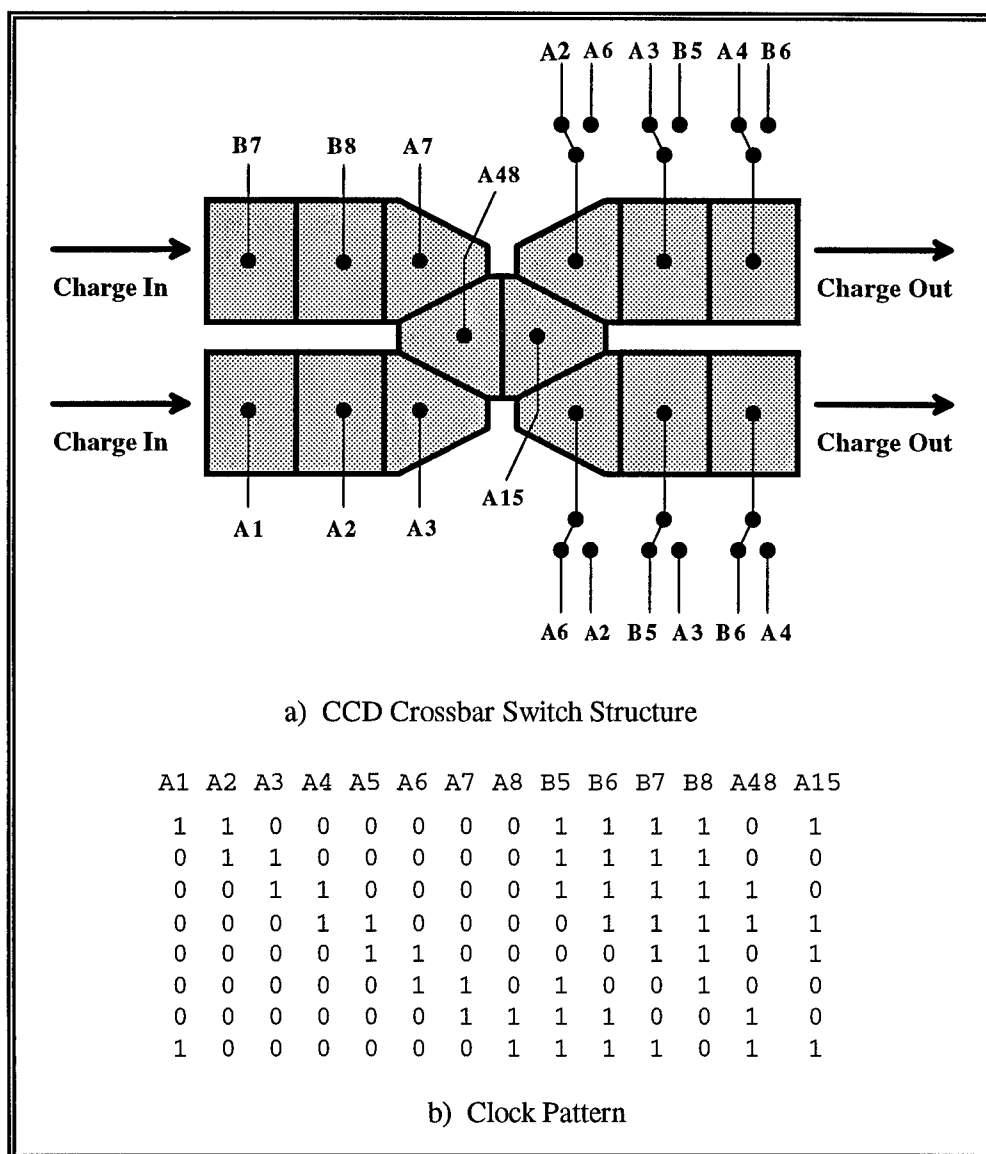


Figure 11: Crossbar Switch

A cartoon illustrating the operation of the crossbar switch in the straight mode is shown in Figure 12. The series of diagrams show an off gate in white, and the on gates in gray, for each clock state in Figure 11b. At the start, Step 0, the two charge packets labeled X and Y are in similar positions on the input side of the crossbar switch. At Step 1, the Y packet begins to advance while the X packet is held stationary. Y continues to advance while X is stationary through Step 4. On steps 5 and 6, both packets advance. For steps 7 through 10, the Y packet is stationary, while X advances. At Step 10, the two packets are again aligned, and are passed out of this structure on Step 11. The two charge packets have been passed straight through the structure, with the X and Y retaining their relative positions top and bottom as they passed through the structure.

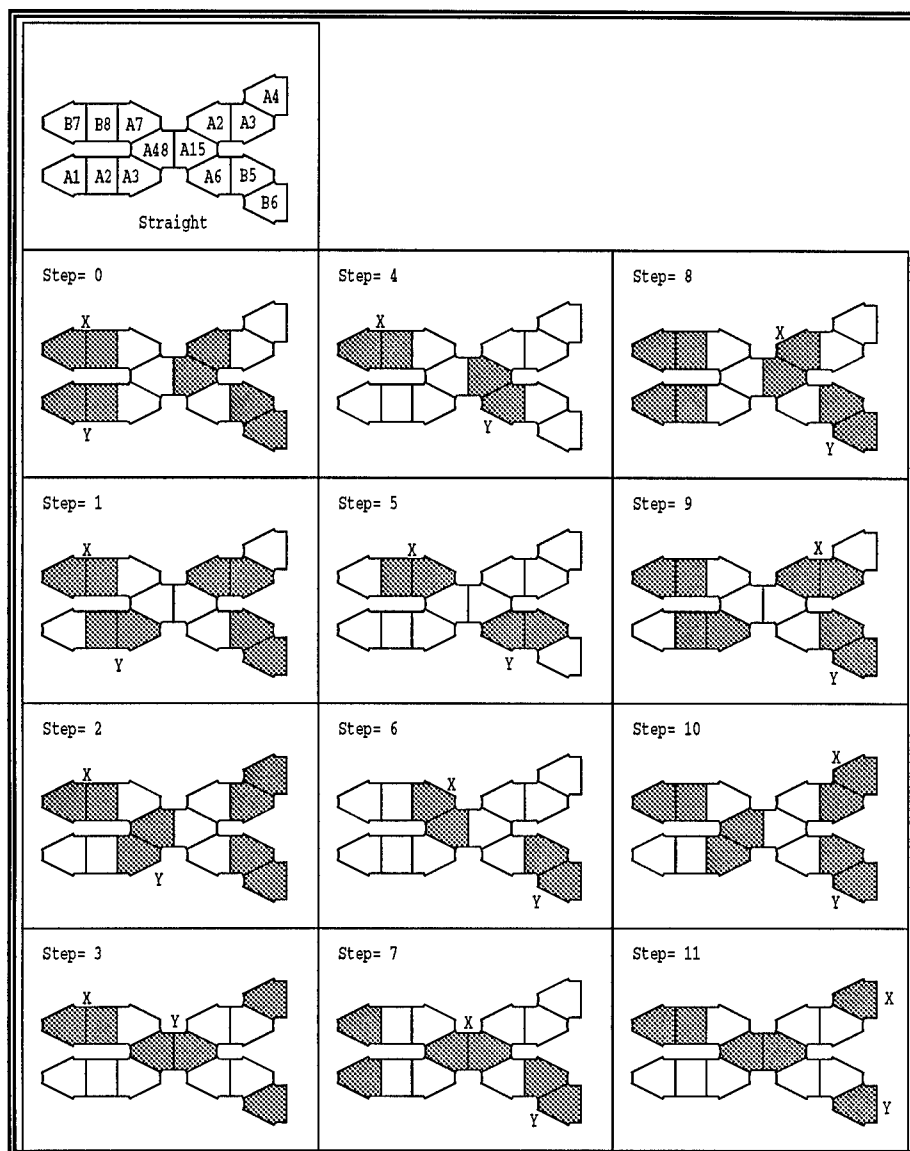


Figure 12: Crossbar Switch in Straight Mode

The cross mode is shown in Figure 13. Operation is identical to the straight mode for Step 0 through Step 3, where the leading Y packet has reached the end of the central electrodes. On Step 4, the Y packet is directed to the top, and on Step 8, the X packet is directed to the bottom, so that at the end Y is on top, and X is on the bottom. The two charge packets have crossed as they passed through the structure, with the X and Y packets exchanging their relative positions.

The clocks repeat in an eight step cycle, so at Step 8 in both Figures 12 and 13 the structure will receive the next pair of charge packets. The delay through the structure shown takes 12 steps, which is 1.5 clock cycles. Additional gates (not shown) increase the delay to an even number of clock cycles.

The clock multiplexers that set the crossbar mode may be switched whenever the pairs of clocks to be exchanged are in the same state in either mode. This eliminates the possibility of switching transients due to clock skew from disrupting the charge. This condition occurs at steps 2 and 3.

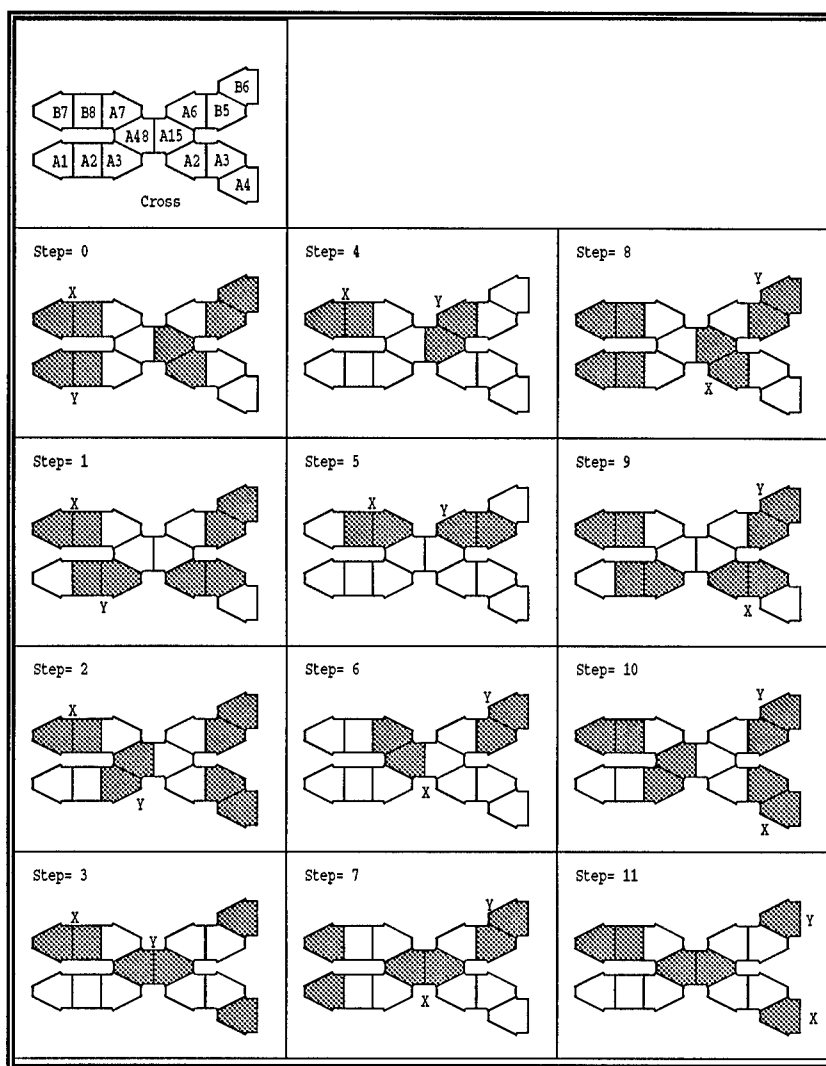


Figure 13: CCD Crossbar Switch in Cross Mode

#### 4.2.4 Quad Sampler

The beamformer must maintain delay resolution of  $\lambda/32$  for a center frequency up to 10 MHz. The delay lines described in the preceding sections could be operated at a 320 MHz clock rate to achieve these goals, but this would make the delay lines too long and would require excessive drive power. A better approach is to have a short, dynamically changeable, delay operating at the high frequency followed by a decimator to reduce the data rate for the remaining delay lines. This will greatly reduce the clock drive power, which is the single largest power consumer in the beamformer. For example, if the data rate is reduced by a factor of four, the clock rate and the number of stages in the following delays will both be reduced by a factor of four. Since the clock drive power is proportional to *both* these parameters, the power will be reduced by a factor of nearly 16. (The gates will have to be slightly larger to maintain the dynamic range, so a full factor of 16 will not be realized.)

A decimation factor of four was chosen for this study. The delay lines will operate at eight times the center frequency, with a Nyquist rate at four times the center frequency. The decimation factor could possibly be increased to eight, yielding a Nyquist rate of two times the center frequency. The impact of increasing the decimation factor will be assessed in Phase II.

The preferred implementation of a quad sampler is shown in Figure 14. A single sampling voltage-to-charge converter operates at the full rate of 320 MHz. The CCD input register continuously shifts the input stream in the direction shown. The four-phase clock uses the sequence P1, P2, P3, P4. At each gate marked P4, the charge will be passed forward or diverted into the output register by clocking the appropriate gate with P1, which will be connected to the gate through a multiplexer (not shown). In this approach, three sequential packets will be diverted and summed in the output register. The remaining samples will be kept in the input register, shifted out and discarded to the sink.

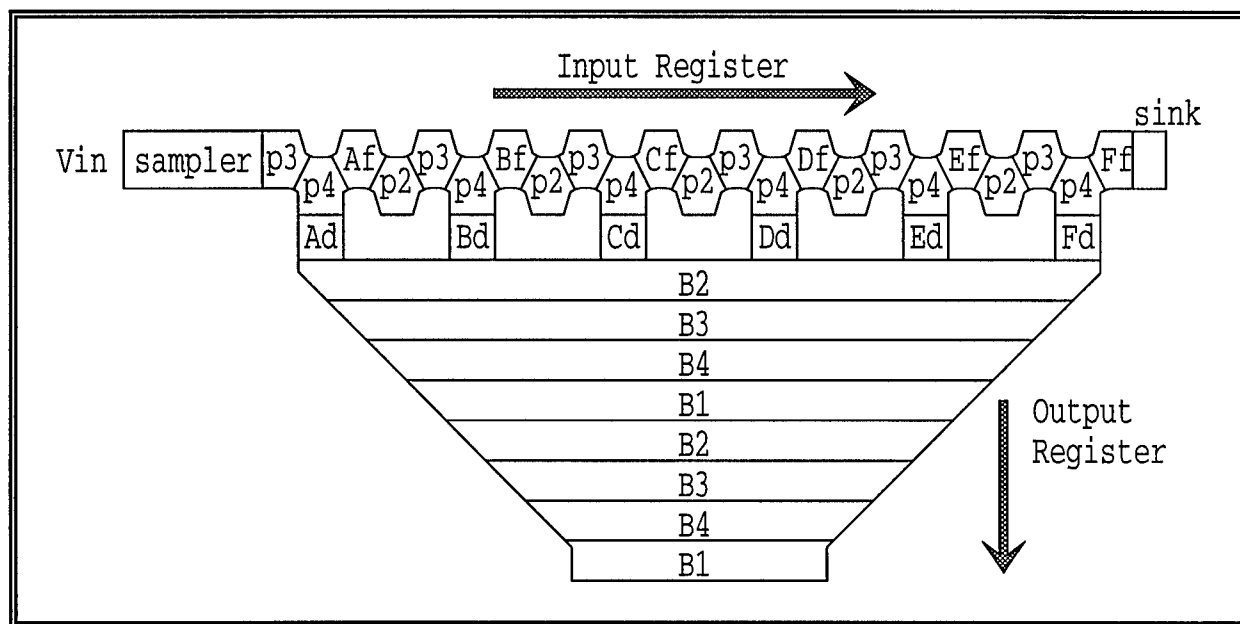


Figure 14: Quad Sampler Structure

The diversion will occur every four cycles of the input register. The output register will cycle at the diversion rate. The group of three stages diverted may be advanced by one stage at any time. As each group of three stages is advanced, the group delay through the quad sampler is increased by the period of one cycle of the input register. Then, the resolution in setting the delay equals the period of the input register clock cycle, or  $\lambda/32$ . After the fourth advance, the diversion is wrapped back to the first group, and the dynamic delay line following the quad sampler is incremented.

This structure could be operated with a single sample instead of summing three samples, but the area of the gates in the input register would have to be increased a factor of three to maintain the dynamic range. The resulting gates would have longer transfer lengths which would seriously degrade the performance of delay line. The summation of the three samples also forms a low-pass filter, which suppresses out-of-band noise which may be aliased into the passband upon decimation.

The operation of the quad sampler is shown in the cartoon of Figure 15. At the start of the cartoon (Step 0), the first three charge samples, Q1, Q2, and Q3, have already been clocked into the input register.

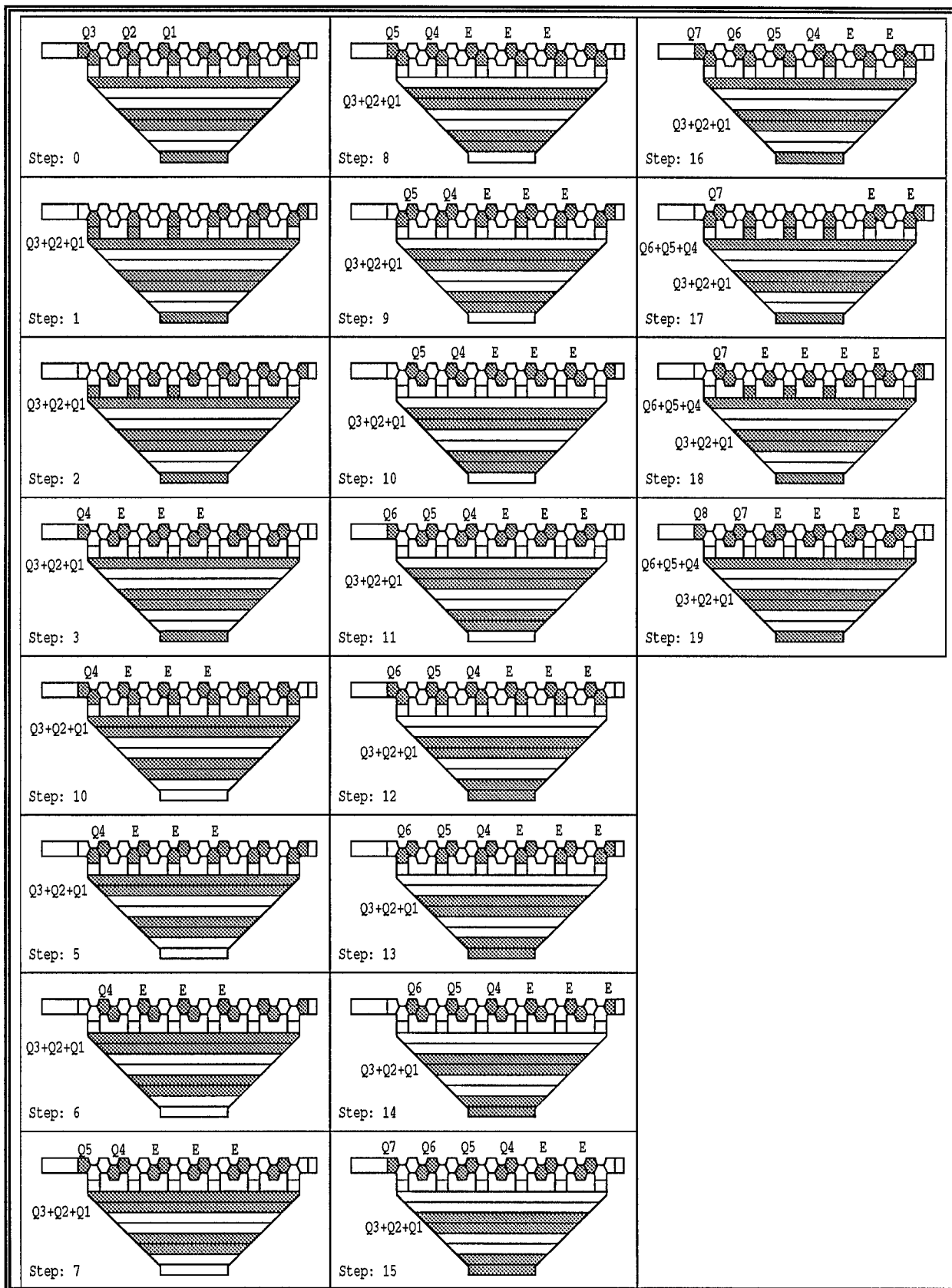


Figure 15: Operation of Quad Sampler



At Step 1, the first three diverters are activated. Three packets flow onto a common gate at the beginning of the output register where they merge into a single packet equal to  $Q1+Q2+Q3$ . Any charge that may have been present in the input register ahead of the diverted packets will be passed forward and eventually discarded in the sink.

At Step 3, the next input sample,  $Q4$ , is placed at the beginning of the input register. The next three stages, marked with an E, are empty, since the charge that otherwise would be located there was diverted into the output register. Charge samples continue to be passed into the input register, so that by Step 16 the register contains samples  $Q4$  through  $Q7$  positioned for the next diversion. At Step 17 the next diversion occurs. Figure 15 illustrates the case where the delay is advanced. The second, third, and fourth diverters are activated so that packets  $Q4$  through  $Q6$  are diverted, summed, and passed to the output register.

Note that if the delay hadn't been advanced, Step 17 would have resembled Step 1, and samples  $Q5$ ,  $Q6$ , and  $Q7$  would be summed. Also, note that if four instead of three samples were summed, the sum at Step 17 would only have three packets ( $Q6+Q5+Q4$ ), since the fourth packet needed ( $Q3$ ) was diverted earlier at Step 1.

This approach has several advantages over other approaches considered. The primary advantage is that there is only one sampler. Other structures might have four samplers, where gain or offset mismatches between the samplers would show up as a fixed pattern noise in the image. Another advantage is that there are no problems with "holes" in the data as the delay is advanced. The third advantage is that the high speed section can be implemented with smaller gates, which improves the transfer performance of the register.

#### 4.2.5 Delay Line Control

The complementary delay line proposed here presents several complicated control issues that have been resolved during Phase I. The two primary difficulties are: 1) controlling the crossbar switches to achieve the appropriate delays, and 2) switching the structure so the sample stream is delayed correctly. As described below, a simple gray code counter solves the first problem, where each bit controls a crossbar switch. By incrementing this counter, the correct delay through the structure is selected. The second problem is much more complex and requires analysis of the position of quad sampler outputs as they progress through the complementary delay. The crux of the problem is that when the quad sampler wraps around from its largest to smallest delay, the complementary delay line should increment its delay by one. However, the samples containing a wrap take time to progress to the crossbar that will repeat one of those samples. As a result, a variable delay must be imposed between a quad sampler wrap and the delay change within the complementary delay line.

The crossbar switches within the delay line are controlled by a gray code sequencer. Each bit controls one switch. The control sequences for a 2-, 3-, 5-, and 9-element delay structure are given in Figure 16 below. The generic structure shows that the crossbars may operate in straight or crossed orientations. The specific examples given in Figure 16 of 10 and 15 sample delays are highlighted lightly in the delay structure. Changing from 10 ( $=1+3+5+1$ ) to 11 ( $=2+3+5+1$ ) involves changing the left-most crossbar (highlighted darker). Similarly, changing from 15 to 16 involves changing the third crossbar so the new delay components are  $1+1+5+9=16$ . Increasing the number of crossbars requires proportionally increasing the length of the gray code control sequence.

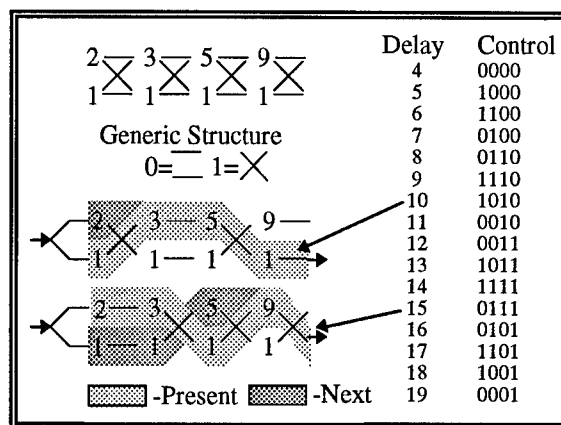


Figure 16: Control Sequences

The quad sampler at the input to the delay line, as described previously, reduces the clock frequency and power consumption of the complementary delay line. It introduces a difficult control issue, however, since switching the quad sample delays must be synchronized with delay line switching. The last sample from the 270° leg must be repeated in the complementary delay line (a +360° change) to compensate for the 270° delay change of the quad sampler. Referring to the lower example in Figure 16, if a sample that needs to be repeated enters the structure at the left, it will take exactly seven cycles before it reaches the crossbar switch (the third one in this case) that repeats that sample and changes the delay from 15 to 16 ( $\lambda/8$ ). The delay from quad sampler wrapping to delay line switching depends exclusively upon which crossbar in the structure will switch to change the delay. Figure 17 presents these delays, termed "geographical offsets" because they are cycle offsets depending on the geographic location of the crossbars within the structure.

Crossbar to Switch	Geographical Offsets
1	2
2	4 = 2*2
3	7 = (4*2)-1
4	12 = (7*2)-2
5	21 = (12*2)-3
6	38 = (21*2)-4
7	71 = (38*2)-5
8	136 = (71*2)-6
9	265 = (136*2)-7

Figure 17: Geographical Offsets

Controlling the switching time of the complementary delay line to within one cycle requires specialized circuitry that tracks how many cycles have elapsed since the quad sampler wrapped. Ideally, this can be done with two counters: one gray code counter provides the control bits to the delay line, and the other counter counts down the geographic offsets before applying this new gray code to the delay line. When the quad sampler wraps around, an offset (511-N) is loaded into the counter. Simultaneously, the gray code counter increments; however, a register withholds this change from the delay line. When the terminal count (511) has been reached, an overflow signal stops the binary counter and allows the new gray

code to be latched into the register driving the delay control lines. The gray code counter provides the offsets with the toggle control bits generated within the counter to indicate which bit will change on the next clock. Only one of the nine T outputs will be high, since only one bit changes for each delay control code.

The control scheme presented above would work well if the frequency of delay changes were very low relative to the frequency that samples move through the structure. In that case, repeated samples would always have a chance to propagate through the structure before another sample must be repeated. Here, however, the delay clock (that moves the samples along) is  $8f_0$  and the fastest the quad sampler will wrap is  $f_0/4$ ). In the worst case, therefore, input samples must be repeated (i.e., the delay must change) every 32 samples. If one of the larger offsets is being counted (e.g., 38, 71, 136, or 265) at least one other offset will need to be considered simultaneously. A second counter is needed to accommodate the situation where a large offset is followed closely by another smaller one. The modified control circuitry is presented below in Figure 18.

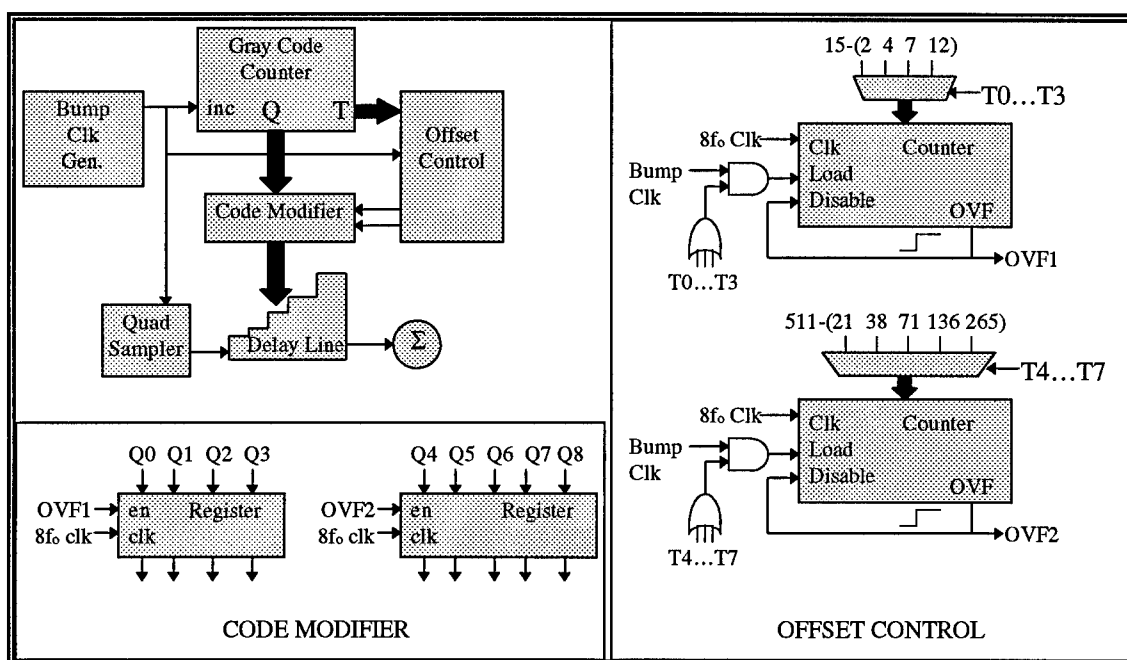


Figure 18: Modified Control Circuitry

When a bit in the control code to the delay line changes, the sample at the appropriate crossbar is repeated. For the case where there are two offsets being counted simultaneously, the control code for the delay line deviates from the normal gray code sequence. Essentially, the bits representing the offset must not change until that offset has expired. The registers in the code modifier are disabled when the corresponding offset is being calculated (i.e., the counter is running). Therefore, the new piece(s) of the gray code from the counter is(are) held off from the delay line until the appropriate binary counter reaches its terminal count and enables the code modifier register(s) to load. Note that simultaneous expiration of the offset counters is not a problem here; however, two crossbars will change in the same cycle to correctly delay the sample stream.

The bump clock generator shown in Figure 19 is a simple computational engine that creates a pulse that follows the  $1/R$  relation for maintaining an in-focus dynamic receive beam. The delays can be changed as quickly as once every range clock cycle, which is set by a minimum  $f/\text{number}$  criterion (2 in this case). The bump clock generator solves the equation:

$$\Delta = \frac{n_0 + \Delta n}{n_0 - m - 1},$$

where  $\Delta$  is the number of range clocks between delay changes,  $n_0$  is the number of range clock cycles from the start of a beam to when the element turns on (for apodization),  $\Delta n$  is the number of range clock ticks since turn on, and  $m$  is the delay change index. The constant  $n_0$  is calculated from various operating parameters such as sample rate, range clock rate, element position, and steering angle. A simple algorithm that solves this equation is shown in Figure 19. The value of  $B$  represents  $n_0 + \Delta n$  and  $A$  represents  $n_0 - m - 1$ .  $C$  is used to calculate how many times  $A$  goes into  $B$ , because  $\Delta = B/A$ .  $C$  also keeps track of remainders. When the appropriate number of inter-bump range clock cycles have elapsed (i.e.,  $\Delta$ ), another bump will be generated.

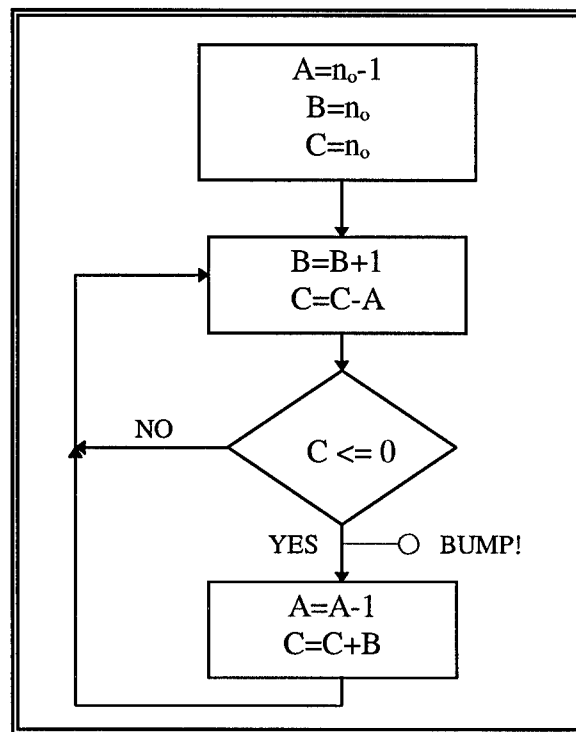


Figure 19: Bump Clock Generator

#### 4.2.6 Prototype Element Fabrication

A test chip is being fabricated to verify the operation of several of the basic CCD elements described in this report. Tests of these elements will verify the functionality and performance of the elements. This test chip was laid out according to the design rules dictated by the foundry fabricating the device. These design rules, which dictate such layout details as minimum mask feature widths and

spacings, have a major impact on size, and, hence, the performance of the elements. It is therefore necessary to actually lay out the critical parts of the beamformer to make realistic predictions of the device performance.

A plot of the masks for the test chip is shown in Figure 20. There are three test structures. The first, magnified in Figure 21, is the crossbar switch described previously, with separate input and output structures. The clock multiplexers are included. Tests of this element will show dynamic range, crosstalk, and any switching upsets.

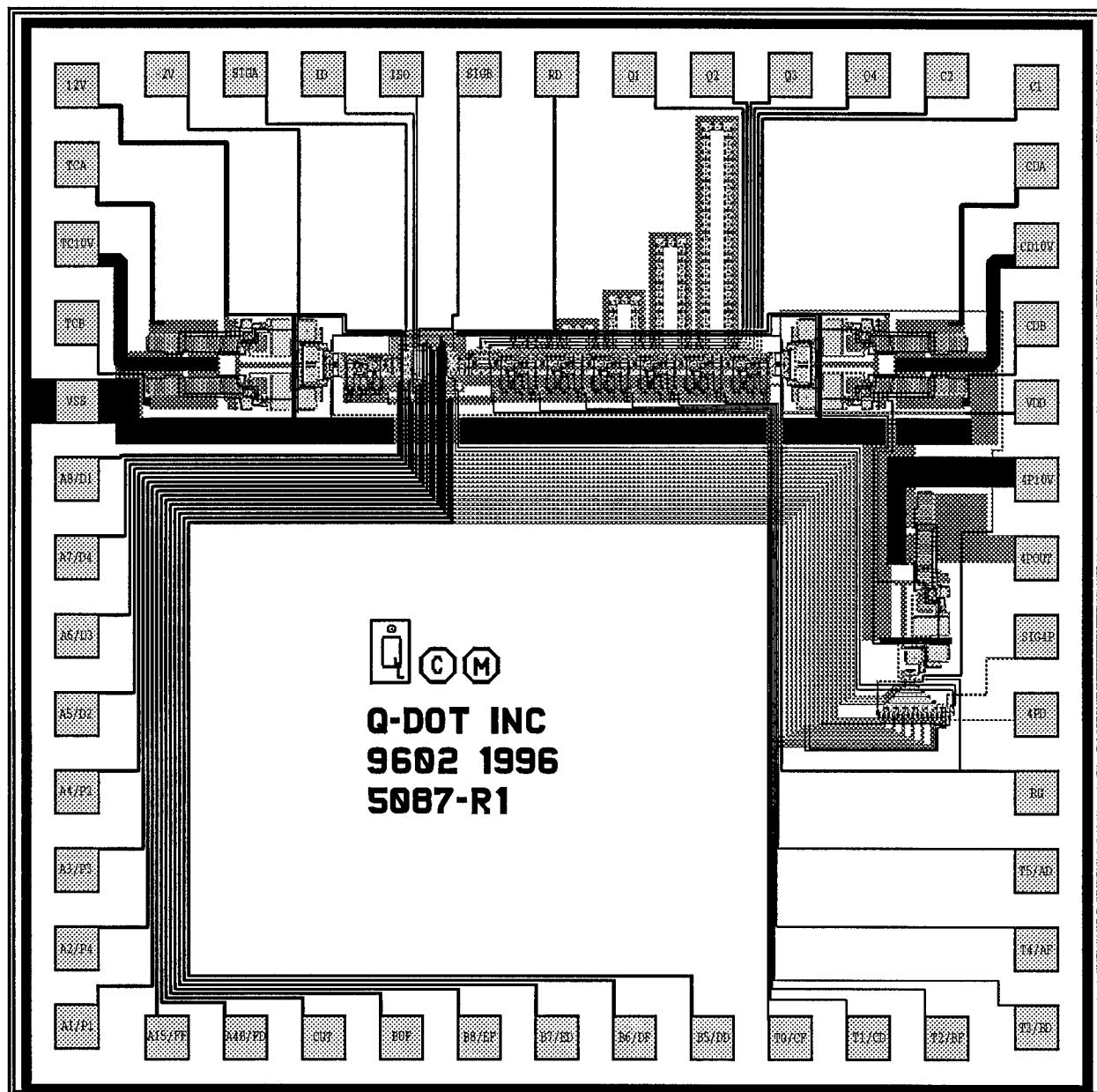


Figure 20: Beamformer Test Chip Mask

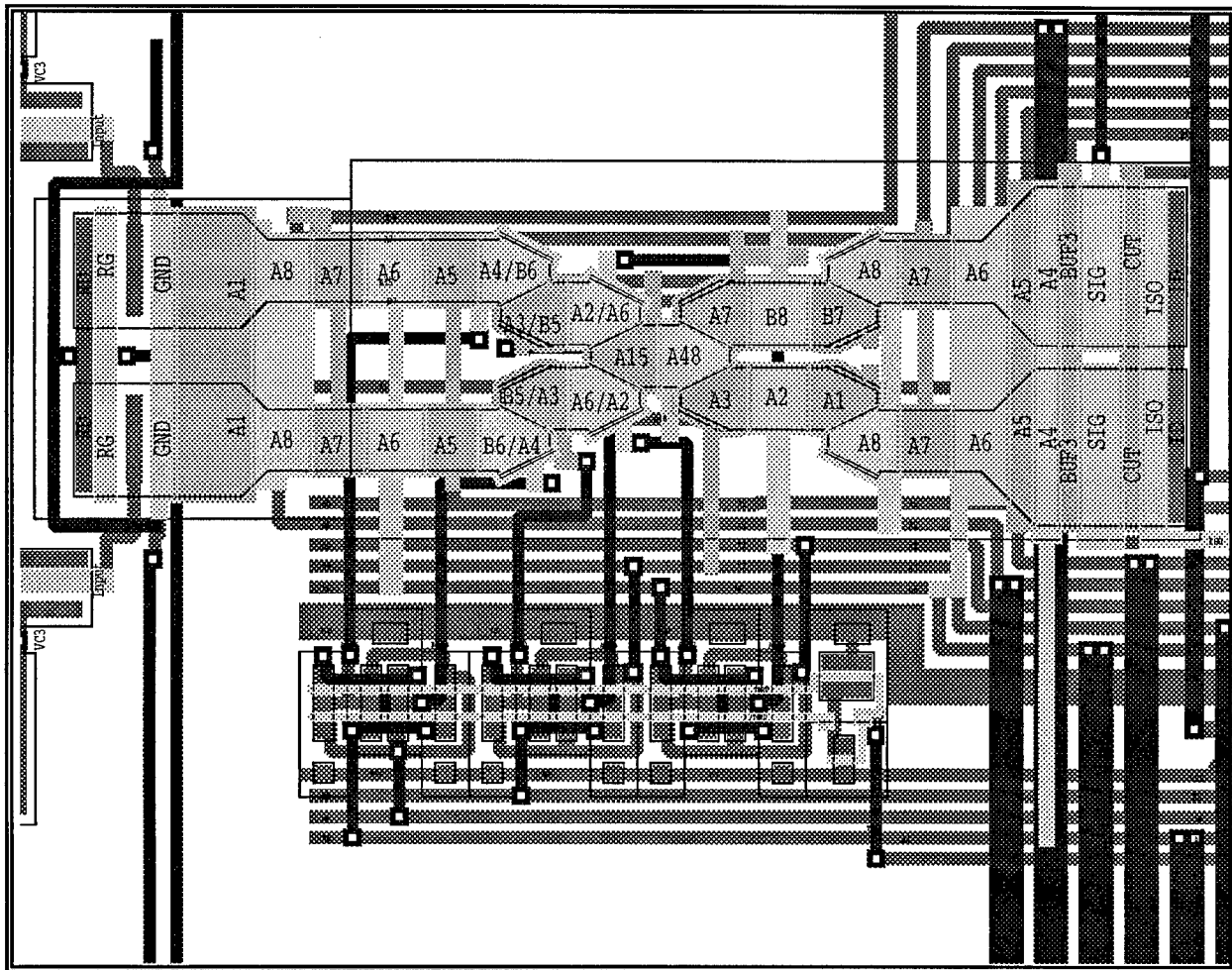


Figure 21: Crossbar Switch Test Element

The second structure, magnified in Figure 22, is a six-loop, complementary delay line with a maximum programmable delay of 64. This is the dynamic delay range of the fine delay identified in the system requirements. In the test element, a single input structure is followed by a charge splitter to make the two inputs to the complementary delay. Separate output buffers are provided. Tests of this element will show dynamic range, crosstalk, switching effects, and charge transfer efficiency effects of the delay line.

The third structure, the quad sampler described earlier, is shown in Figure 23. A single input structure and output buffer are provided. Tests will show dynamic range, and will identify the clock voltages needed for correct operation.

#### 4.3 Potential Performance Limiting Factors

As the beamformer design evolved, several factors were considered which appeared capable of limiting beamformer and/or scanner performance. Three such factors were analyzed: charge transfer efficiency, dynamic range, and power consumption. The following subsections address each of the factors individually.

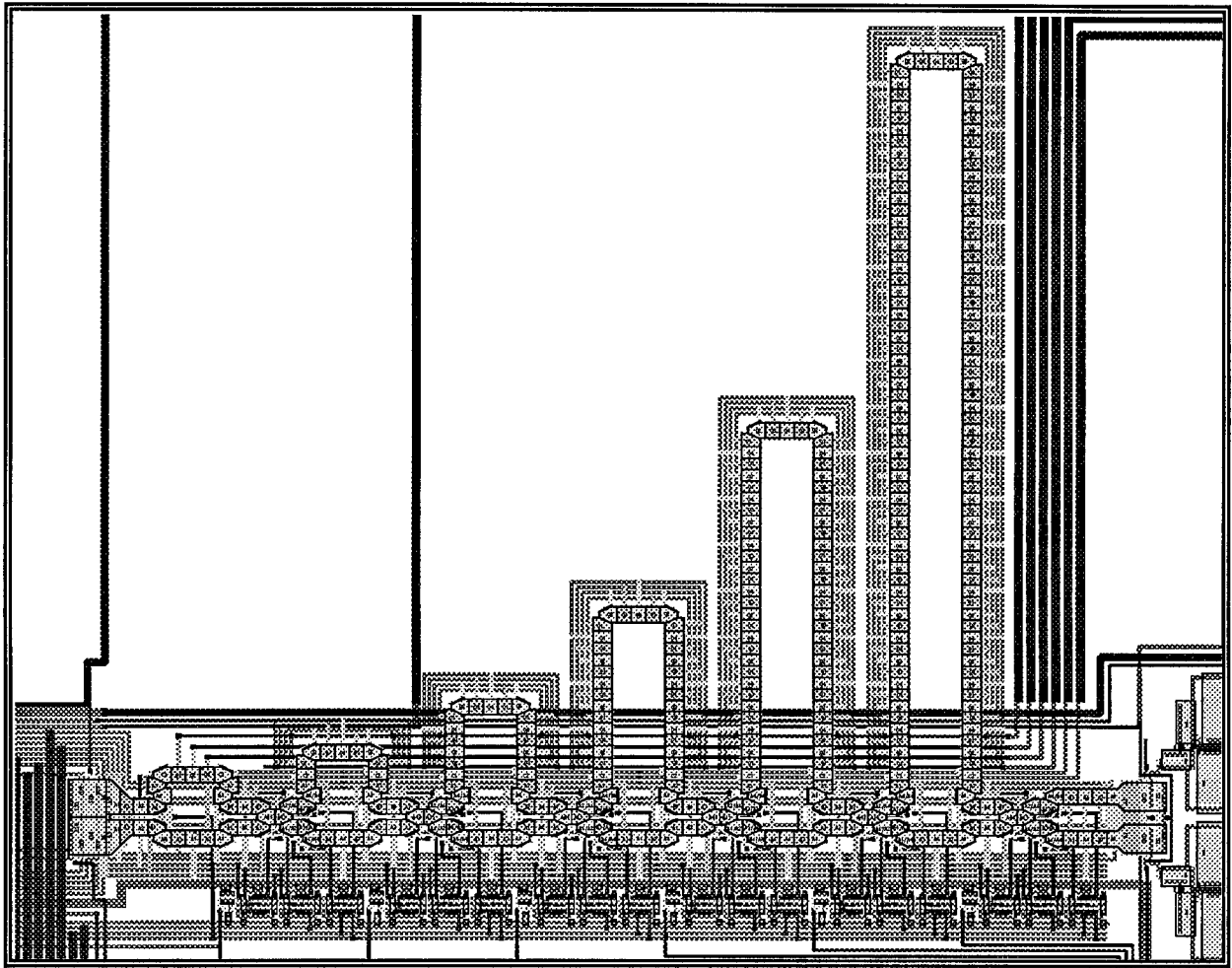


Figure 22: Complementary Delay Line Test Element

#### 4.3.1 Charge Transfer Efficiency Effects

Incomplete charge transfer between adjacent CCD gates modifies the charge packet stream. A small fraction of each packet is left behind as charge is shifted along the structure. The charge left behind combines with other charge packets later occupying the same potential well under the CCD gate. This charge sharing is characterized by a numerical fraction of the charge fed forward, and is called charge transfer efficiency (CTE). CTE varies dramatically between different CCD structures and processes. Buried-channel CCDs (like the ones used on this project) have by far the best CTE because the charge-carrying potential well lies below the surface of the silicon-oxide interface and thereby avoids charge-trapping surface states. Although CTE values of greater than 0.999 are expected for the proposed project, process variations or increased operating frequencies could reduce the CTE to 0.997. A worst case CTE of 0.995 will be used for investigating its effects on the proposed beamforming system. Although it is unlikely that charge transfer efficiency will be this poor, it is useful to investigate its effect on imaging.

A charge packet in a realistic CCD is a combination of the current charge packet together with ever decreasing contributions from those packets that have come before. The  $N^{\text{th}}$  packet, for instance, has the following characteristic after being fed forward once:

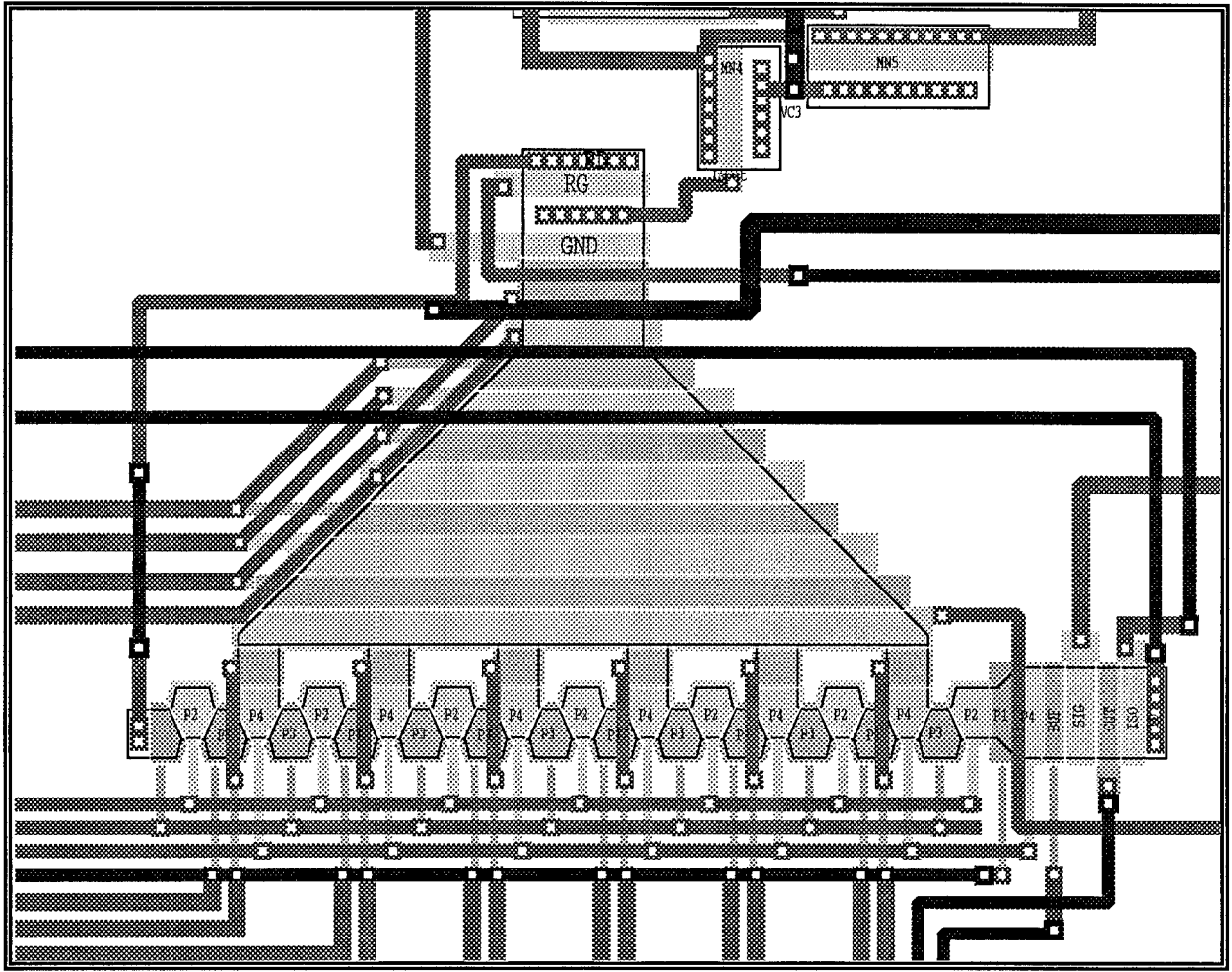


Figure 23: Quad Sampler Test Element

$$V_N((n+1)\tau) = (1-\epsilon)V_{N-1}(n\tau) + \epsilon V_N(n\tau),$$

where  $V_N$  is the voltage under the  $N^{\text{th}}$  gate,  $1-\epsilon$  is the CTE, and  $n\tau$  is the clock index. The  $(1-\epsilon)V_{N-1}(n\tau)$  term represents the value of the current packet just fed forward, whereas  $\epsilon V_N(n\tau)$  is that portion of the previous packet left behind. Taking a Z-transform and combining the  $\epsilon$ -related terms into a dispersion factor  $D(z)$ , we have:

$$V_N(z) = [(1-\epsilon)/(1-\epsilon z^{-1})]z^{-1}V_{N-1}(z) = D(z)z^{-1}V_{N-1}(z).$$

For  $M$ , such transfers the dispersion factor is raised to a power  $M$ , as is the delay factor  $z^{-1}$ :

$$H(z) = [(1-\epsilon)/(1-\epsilon z^{-1})]^M z^{-M} = D^M(z)z^{-M}.$$

This can be expanded to:

$$H(z) = \sum_{n=0}^{\infty} \binom{M+n-1}{n} \epsilon^n (1-\epsilon)^M z^{-(M+n)}$$



which is just a filter acting on the input data stream. This filter is phase-linear and low-pass in nature and rolls off quickly for very large values of  $M$ , which would occur in very long CCD structures.

To understand CTE effects on image quality, we have simulated CTE losses within the delay structures of the system by calculating the appropriate filters and applying them to the sampled ultrasound RF signals. Figure 24 shows the Fourier Transform of a single channel RF pulse for the wire target phantom ( $f_0 = 3.4$  MHz,  $f_s/4 = 108/4 = 27$  MHz). The noise floor is visible approximately 60 dB down from the ultrasound carrier frequency components. Superimposed on this graph is the CTE ( $= 0.995$ ) filter frequency response due to 512 and 250 charge transfers. This figure shows that the oversampling imposed by the system to achieve sufficient delay accuracy also allows the imaging frequencies to lie within the passband of the CTE filter. Some attenuation will occur for elements undergoing large delays (e.g., 512 transfers). Others, however, will have little, if any, delay, so the effects of CTE attenuation will be minimal. A group delay will also be imposed by the CTE filter and has the potential to disrupt some of the dynamic focusing of the system. Static group delays (i.e., delays due to large steering angles), however, can be compensated by beamforming software.

Figures 25 and 26 present 70 dB ultrasound images of wires in a water tank produced by the proposed system. Figure 25 does not take into account charge transfer efficiency effects, whereas, Figure 26 has a CTE of 0.995. Very little difference between these two images is apparent. Actually the central portions of these two images are almost identical because the number of delays imposed on the signals are small due to the near-zero steering angle. There is a very slight reduction in the peak wire intensities throughout Figure 26, due to CTE filter attenuation as well as group delay defocusing effects which were not corrected.

Figures 27 and 28 present 50 dB ultrasound images of a phantom with randomly distributed scatterers everywhere except within four cylindrical anechoic (i.e., cyst) regions visible in the images. There are no noticeable differences between Figure 27, which does not account for CTE effects, and Figure 28 which has a CTE of 0.995 imposed.

These simulations show that the effects of charge transfer efficiency within the CCD delay line (down to 0.995) have minimal effect on image quality. Attenuation effects of CTE are minimized due to the oversampling ratio of the system, however, some attenuation does occur. Processing across the array also reduces CTE effects because every beam sums elements with large and small delays imposed, averaging the overall attenuation. Additionally, the group delay imposed by the filter apparently does not greatly affect the focusing ability of the beamformer. Even if it did, the control circuitry of the beamformer could easily be programmed to take these dispersion effects into account.

Expected charge transfer efficiencies for this project range from 0.999 to 0.9999. These simulations show that the beamformer could tolerate a poor 0.995 CTE without noticeable image degradation. Charge transfer effects, therefore, are not considered to be a significant technical challenge for this project.

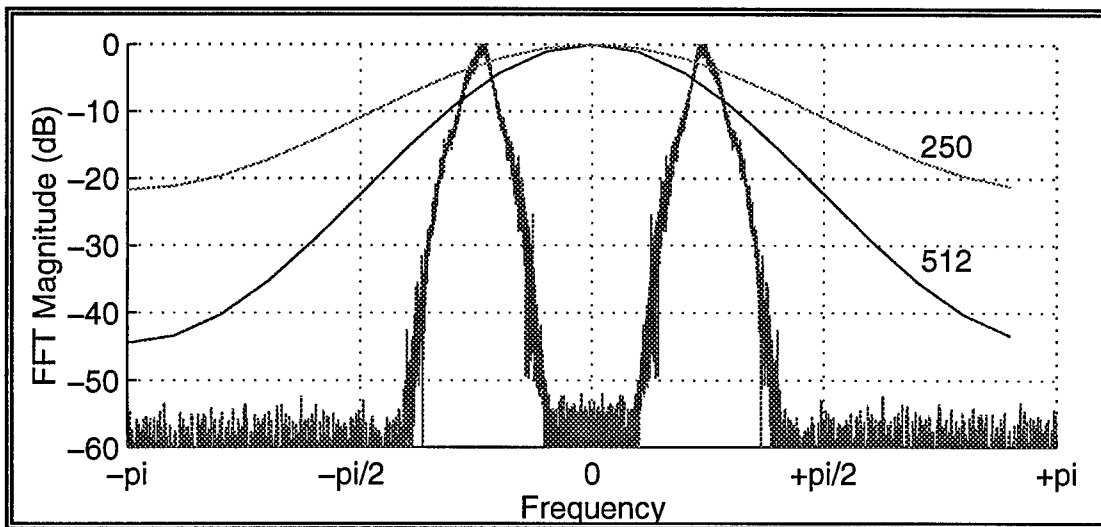


Figure 24: Fourier Transform of Wire Target

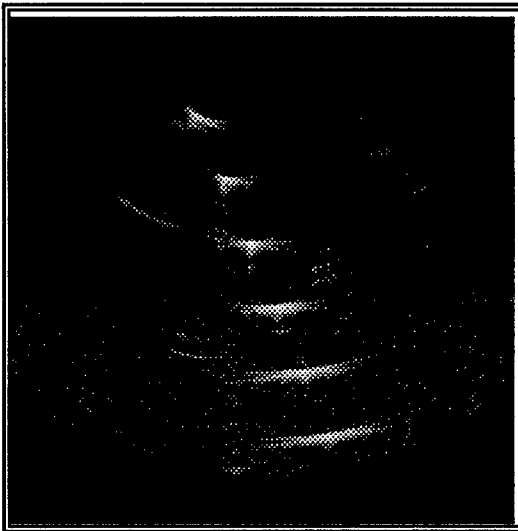


Figure 25: Wires, No CTE Effects



Figure 26: Wires, CTE = 0.995

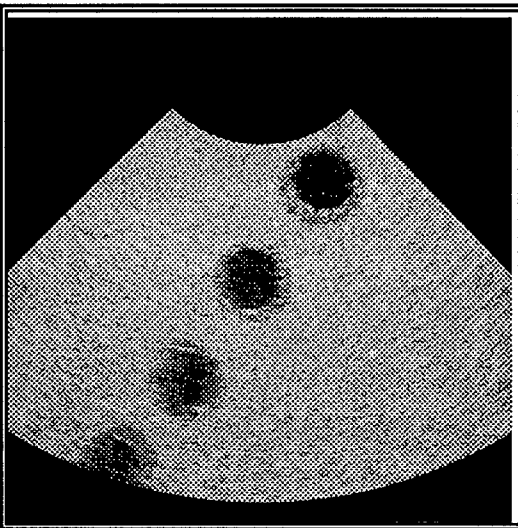


Figure 27: Cyst Phantom, No CTE Effects

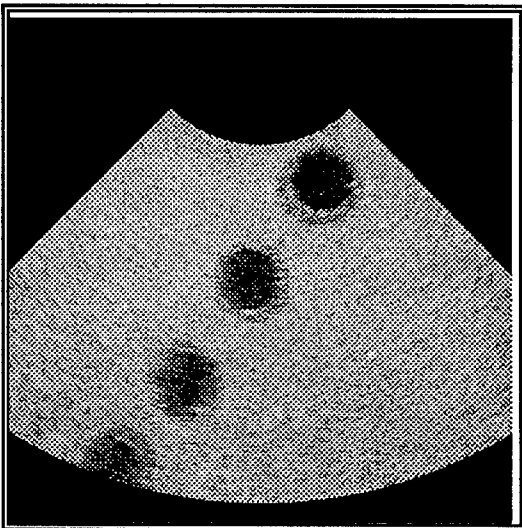


Figure 28: Cyst Phantom, CTE = 0.995

### 4.3.2 Dynamic Range

The dimensions of the gates used in the delay lines have a drawn area of approximately  $100 \mu\text{m}^2$ . Fringing and the impingement of field oxide into the channel reduce the effective area to  $75 \mu\text{m}^2$ . The buried-channel implants result in a maximum charge density of  $3.3 \times 10^{11}$  electrons/ $\text{cm}^2$  which corresponds to a maximum signal swing of 240,000 electrons peak-peak, or 85,000 electrons RMS for a sine wave. The effective capacitance of the input signal gate is  $2.8 \times 10^{-8}$  F/ $\text{cm}^2$ , which yields an input capacitance of  $C_{\text{in}} = 20$  fF. The charge is sensed on an output diffusion which is computed to have a capacitance of 12 fF.

The noise generated in the CCD input circuit is expected to consist of the so called "kTC" noise, which results in a total noise charge at the CCD output of  $(kT(C_{\text{in}} + C_{\text{out}}))^{1/2} = 72$  electrons RMS. The output buffer degrades the noise by approximately 1 dB, yielding a net channel dynamic range of 60.5 dB. The processing gain that results from summing 64 channels adds 18 dB, which gives the overall dynamic range of 78.5 dB. This performance meets the system requirements identified in Section 4.1.

### 4.3.3 Power Consumption

The power needed to operate the CCDs is actually consumed in the clock drivers. When each clock line is pulled positive, the charge on the capacitance of the line flows as current from the positive power supply. The energy stored on the clock line capacitance is dissipated when the voltage is pulled negative. The power consumed in the driver is given by

$$P = 1.5CV^2f$$

where 1.5 is the driver efficiency,  
C is the clock line capacitance,  
V is the change in voltage (5V),  
and f is the average frequency.

Total clock line capacitance for a channel consisting of a four-phase sampler, and a 512-stage complementary delay line is 58 pF, in a section operated at a maximum of 80 MHz, and 0.8 pF in a section operated at 320 MHz. The driver power will be 185 mW. Note that this power is proportional to the sampling rate, which is related to the detector frequency. For the minimum specified center frequency, 2.5 MHz, the power will be reduced to 46 mW.

The output buffer is estimated to require between 20 and 30 mW, per channel, making the total channel power 215 mW, worst case.

If the four-phase sampler proposed is replaced by an eight-phase sampler, the maximum CCD clock rate is reduced to 40 MHz, and the delay line requires only 256 stages. In this case, the clock line capacitance becomes 32 pF operated at a maximum of 40 MHz, and 1.4 pF operated at 320 MHz. The maximum driver power will then be 65 mW. The impact on other aspects of the beamformer will be thoroughly assessed before making this change. Other techniques for reducing power will be considered in Phase II.

#### 4.4 Phase II Development Plan

Q-DOT proposes to provide all labor, materials, services, and communication necessary to develop a low-cost, low-power, high-performance beamformer based on CCD/CMOS technology. Matthew O'Donnell, Professor of Electrical and Computer Science at the University of Michigan and a world-class designer of medical ultrasound systems, will guide Q-DOT's beamformer design, drawing on his extensive experience in related systems. Q-DOT's plan to develop the proposed beamformer chip is diagrammed in Figure 29, the Phase II Work Plan.

Q-DOT also proposes an Optional program to demonstrate the beamformer chip. The plan for the demonstration Option is shown in Figure 30. Details of the two work plans are presented in the Appendix.

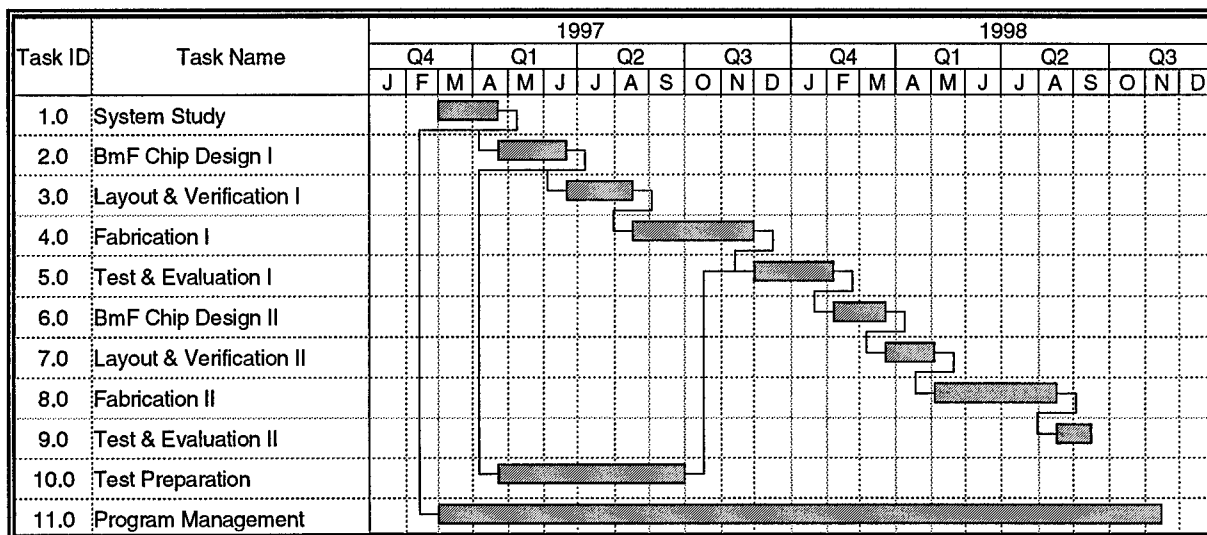


Figure 29: Phase II Work Plan

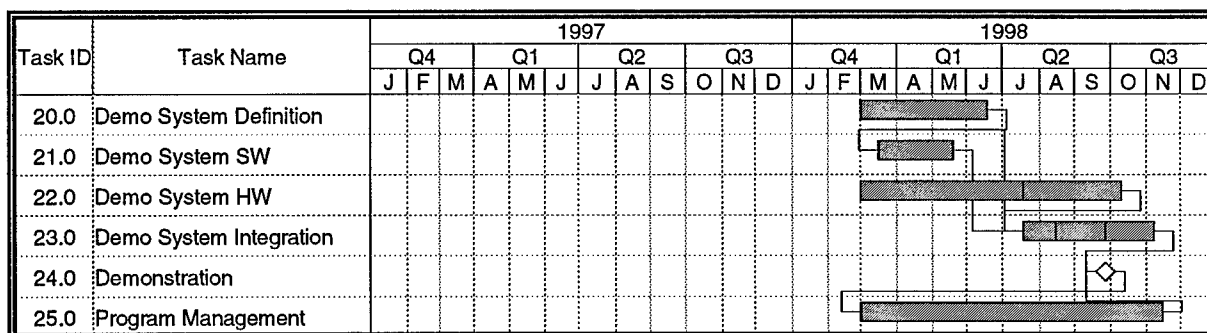


Figure 30: Phase II Option Work Plan

## Task 1            System Study

The requirements defined under Phase I will be fleshed out to include such matters as the exact functions and interfaces to the beamformer chip. This task will result in a complete specification for the beamformer chip.

## Task 2            Beamformer Chip Design I

Given the specification from Task 1, we will design the details of the various sections of the beamformer chip. The apodizer, which was not investigated in Phase I, will be based on a design developed at Q-DOT on another program. Both digital and analog simulations will be performed to assure that the design will meet the specifications.

## Task 3            Layout and Verification I

The actual layout of the beamformer chip will be done in Task 3. We will verify the layout using computer aided design (CAD) software. Critical functions will be broken out into separate test cells.

## Task 4            Fabrication I

The chip will be combined on a mask set with one or more designs from other projects for fabrication at an outside foundry. The cost sharing from this multiproject approach will reduce the cost to this particular program.

## Task 5            Test and Evaluation I

The chip will be tested against the specification developed in Task 1. Critical test elements will be tested as needed to isolate any problems or performance issues.

## Task 6            Beamformer Chip Design II

## Task 7            Layout and Verification II

## Task 8            Fabrication II

## Task 9            Test and Evaluation

A second pass at the chip design, layout, fabrication, and test is planned to correct any problems with the first pass design. We consider a second pass to be necessary for an analog chip of this complexity.

## Task 10           Test Preparation

A custom test fixture will be designed and built under this task. We will develop custom software to control the tests, and manage the resulting data.

## Task 11           Program Management

Program management continues throughout the duration of the project. We will generate a comprehensive final report at the conclusion of this task.

## Optional Demonstration Project

The optional demonstration project will use the beamformer chips, with an ultrasound probe, preamplifiers, and TGC to acquire ultrasound data in real time. The stored data will be processed off-line to generate several sequential frames of ultrasound images for display. The demonstration will use a transducer probe from a commercially available ultrasound system with characteristics similar to the proposed system.

### Task 20 Demonstration System Definition

The requirements on the hardware for the demonstration system will be developed under this task. We will design and build the analog front-end consisting of the preamplifiers, time gain control, transmit/receive switches, and drivers.

### Task 21 Demonstration System Software

At the start of this task, we will define the software to control the beamformer in real time, and for off-line video processing. We will develop this software in conjunction with the University of Michigan.

### Task 22 Demonstration System Hardware

The frame grabber will be developed under subcontract to the University of Michigan.

### Task 23 Demonstration System Integration

Once the first-pass beamformer chips are evaluated, we will combine the probe, front-end, control software and off-line software to make the complete demonstration system. We are assuming that the first-pass beamformer chips will be functional, so that the integration and debug of the demonstration system may be completed by the time the final chips are ready.

### Task 24 Demonstration

The system will be demonstrated for our sponsors and interested industry personnel.

### Task 25 Demonstration Program Management

The results of the demonstration project will be summarized in a comprehensive final report.

## 5.0 Conclusions

It is feasible to realize a multichannel beamformer based on CCD technology for a portable ultrasound system having performance comparable to the current commercial state of the art. The power consumption will be 10% of conventional digital techniques, so battery powered operation is feasible. Dynamic range will be adequate for sensitive color flow images and duplex Doppler measurements. A major limitation in the use of CCD delay lines, charge transfer efficiency, will have negligible effects on image quality. A chip containing critical test elements is being fabricated.

## Appendix -- Phase II Work Plan Detail

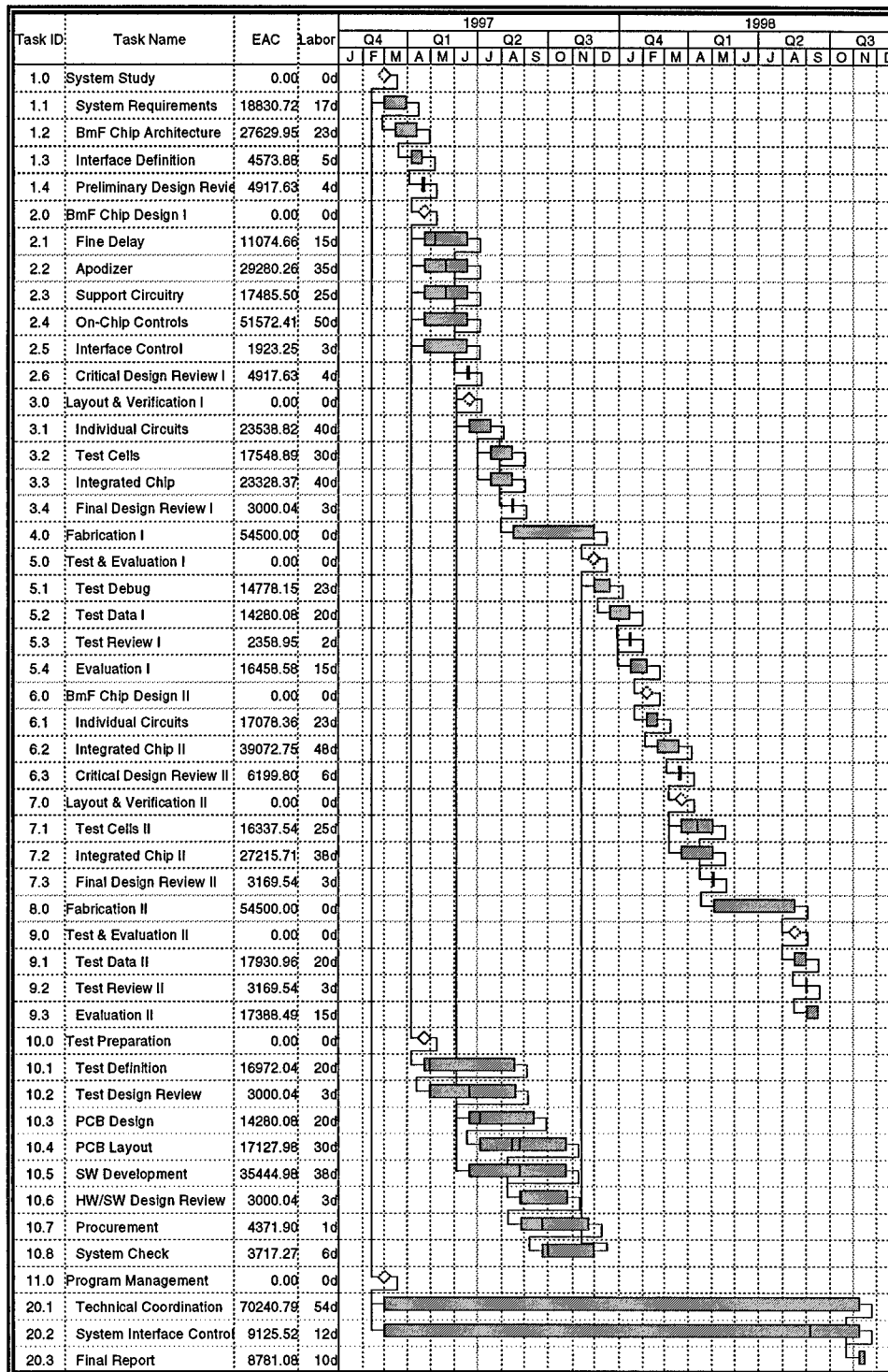


Figure 31: Phase II Work Plan Detail





Personnel Who Received Compensation  
for Work Performed Under Contract DAMD17-96-C-6037

*Q-DOT, Inc.*

Thomas E. Linnenbrink, Principal Investigator

Marshall K. Quick

Guy F. Vanstraelen, Ph.D.

Elizabeth E. Brewer

Cheryl L. Ernst

Jennifer D. Muir

J. Renae Woody

*University of Michigan  
Biomedical Ultrasonics Laboratory*

Professor Matthew O'Donnell

Steven R. Freeman





DEPARTMENT OF THE ARMY  
US ARMY MEDICAL RESEARCH AND MATERIEL COMMAND  
504 SCOTT STREET  
FORT DETRICK, MARYLAND 21702-5012

REPLY TO  
ATTENTION OF:

MCMR-RMI-S (70-1y)

4 Dec 02

MEMORANDUM FOR Administrator, Defense Technical Information  
Center (DTIC-OCA), 8725 John J. Kingman Road, Fort Belvoir,  
VA 22060-6218


SUBJECT: Request Change in Distribution Statement

1. The U.S. Army Medical Research and Materiel Command has reexamined the need for the limitation assigned to technical reports written for this Command. Request the limited distribution statement for the enclosed accession numbers be changed to "Approved for public release; distribution unlimited." These reports should be released to the National Technical Information Service.

2. Point of contact for this request is Ms. Kristin Morrow at DSN 343-7327 or by e-mail at Kristin.Morrow@det.amedd.army.mil.

FOR THE COMMANDER:

Encl

  
PHYLLIS M. RINEHART  
Deputy Chief of Staff for  
Information Management

ADB218773	ADB229914
ADB223531	ADB229497
ADB230017	ADB230947
ADB223528	ADB282209
ADB231930	ADB270846
ADB226038	ADB282266
ADB224296	ADB262442
ADB228898	ADB256670
ADB216077	
ADB218568	
ADB216713	
ADB216627	
ADB215717	
ADB218709	
ADB216942	
ADB216071	
ADB215736	
ADB216715	
ADB215485	
ADB215487	
ADB220304	
ADB215719	
ADB216072	
ADB222892	
ADB215914	
ADB222994	
ADB216066	
ADB217309	
ADB216726	
ADB216947	
ADB227451	
ADB229334	
ADB228982	
ADB227216	
ADB224877	
ADB224876	
ADB227768	
ADB228161	
ADB229442	
ADB230946	
ADB230047	
ADB225895	
ADB229467	
ADB224342	
ADB230950	
ADB227185	
ADB231856	